ON TIME ANALYSIS OF ARCHAEOLOGICAL RESIDUES BY USING LASER-INDUCED BREAKDOWN SPECTROSCOPY(LIBS)

A THESIS SUBMITTED TO
THE GRADUATE SCHOOL OF NATURAL AND APPLIED SCIENCES
OF
MIDDLE EAST TECHNICAL UNIVERSITY

BY

EFE KÜÇÜKKESKİN

IN PARTIAL FULFILLMENT OF THE REQUIREMENTS
FOR
THE DEGREE OF MASTER OF SCIENCE
IN
PHYSICS

AUGUST 2016

Approval of the thesis:

ON TIME ANALYSIS OF ARCHAEOLOGICAL RESIDUES BY USING LASER-INDUCED BREAKDOWN SPECTROSCOPY(LIBS)

submitted by **EFE KÜÇÜKKESKİN** in partial fulfillment of the requirements for the degree of **Master of Science in Physics Department, Middle East Technical University** by,

Prof. Dr. Gülbin Dural Ünver
Dean, Graduate School of **Natural and Applied Sciences** ______________

Prof. Dr. Sadi Turgut
Deputy Head of Department, **Physics** ______________

Assoc. Prof. Dr. Burak Yedierler
Supervisor, **Physics Department, METU** ______________

Asst. Prof. Dr. Kemal Efe Eseller
Co-Supervisor, **Electrical and Electronics Engineering Dept., Atılım University** ______________

Examining Committee Members:

Prof. Dr. Enver Bulur
Physics Department, METU ______________

Assoc. Prof. Dr. Burak Yedierler
Physics Department, METU ______________

Assoc. Prof. Dr. Serhat Çakır
Physics Department, METU ______________

Assoc. Prof. Dr. Akın Akdağ
Chemistry Department, METU ______________

Asst. Prof. Dr. Filiz Korkmaz Özkan
Physics Department, Atılım University ______________

Date: 19.08.2016

I hereby declare that all information in this document has been obtained and presented in accordance with academic rules and ethical conduct. I also declare that, as required by these rules and conduct, I have fully cited and referenced all material and results that are not original to this work.

Name, Last name : EFE KÜÇÜKKESKİN

Signature :

ABSTRACT

ON TIME ANALYSIS OF ARCHAEOLOGICAL RESIDUES BY USING LASER-INDUCED BREAKDOWN SPECTROSCOPY(LIBS)

Küçükkeskin, Efe
M.S., Department of Physics
Supervisor : Assoc. Prof. Dr. Burak Yedierler
Co-Supervisor : Asst. Prof. Dr. Kemal Efe Eseller

August 2016, 86 pages

In this study, Laser-Induced Breakdown Spectroscopy (LIBS) was applied to the archaeological rock samples. The main aim of this study is to find out the LIBS spectra of these rock samples and analyze them qualitatively and quantitatively. It was determined as a result of the qualitative analyses that the elements Mg (I) (517 nm), Sr (II) (421 nm) and Cr (I) (428 nm) exist in the archaeological materials. This information was proved not only with the related software program but also comparing our results with the National Institute of Standards and Technology (NIST) database. Moreover, the limit of detection (LOD) values of the elements Mg, Sr and Cr were calculated as 0.02, 0.38 and 1.34 in the unit of mg/kg or ppm respectively and these very low LOD values showed that using LIBS on the rock samples was suitable method. In the quantitative analyses, the calibration curves of these detected elements were constructed to see whether there is a linear fitting or not by observing the variation of the peak intensity or area under peak coming from the LIBS spectra depending on the concentration in the archaeological samples. The calibration technique using the OH emission band area to eliminate the matrix effects was found to be the best solution.

Keywords: Laser-Induced Breakdown Spectroscopy (LIBS), Qualitative and quantitative analyses

ÖZ

LIBS TEKNOLOJİSİ İLE ARKEOLOJİK KALINTILARIN ANALİZİ

Küçükkeskin, Efe
Yüksek Lisans, Fizik Bölümü
Tez Yöneticisi : Doç. Dr. Burak Yedierler
Ortak Tez Yöneticisi : Yrd. Doç. Dr. Kemal Efe Eseller

Ağustos 2016, 86 sayfa

Bu tezde, Lazer İndüklenmiş Plazma Spektroskopisi (LIBS) arkeolojik kaya örneklerine uygulanmıştır. Bu çalışmanın asıl amacı bu kaya örneklerinin LIBS spektrumlarını bulmak ve bu spektrumları niteliksel ve niceliksel olarak analiz etmektir. Niteliksel analizlerin sonucunda 517 nm'deki Magnezyum Bir (Mg (I)), 421 nm'deki Stronsiyum İki (Sr (II)) ve 428 nm'deki Krom Bir (Cr (I)) elementlerinin arkeolojik örneklerde var olduğu belirlenmiştir. Bu bilgi sadece ilgili yazılım programıyla değil aynı zamanda sonuçlarımızın National Institute of Standards and Technology (NIST) veritabanıyla karşılaştırılmasıyla da kanıtlanmıştır. Ayrıca, Mg, Sr ve Cr elementlerinin tespit limiti (LOD) değerleri sırasıyla 0.02, 0.38 ve 1.34 mg/kg veya ppm olarak hesaplanmıştır ve bu çok düşük LOD değerleri gösterdi ki LIBS'i kaya örneklerinin üzerinde kullanmak oldukça uygun bir yöntemdi. Niceliksel analizlerde, LIBS spektrumlarından elde edilen pik şiddetinin ya da pik altındaki alanın arkeolojik örneklerdeki konsantrasyona bağlı değişimini gözlemleyip lineer uygunluk olup olmadığını görmek için bu tespit edilen elementlerin kalibrasyon eğrileri oluşturulmuştur. Matris etkilerini ortadan kaldırmak için OH emisyon bandı alanının kullanıldığı kalibrasyon tekniğinin en iyi çözüm olduğu saptanmıştır.

Anahtar Kelimeler: Lazer İndüklenmiş Plazma Spektroskopisi (LIBS), Niteliksel ve niceliksel analizler

To My Sister

ACKNOWLEDGMENTS

First and foremost, I must thank my supervisor Assoc. Prof. Dr. Burak Yedierler and co-supervisor Asst. Prof. Dr. Kemal Efe Eseller for their supervision, guidance, advice, criticism, encouragement and patience throughout this study. It was honor for me to be accepted into their research group at the beginning of my first graduate year in the Department of Physics at Middle East Technical University. I have learned precious knowledge since I work with them and I hope this will continue flawlessly.

I would also like to thank Prof. Dr. Sinan Bilikmen and Assoc. Prof. Dr. Serhat Çakır for their unending support to me and my studies.

Additional thanks to Prof. Dr. Enver Bulur, Assoc. Prof. Dr. Akın Akdağ and Asst. Prof. Dr. Filiz Korkmaz Özkan for serving on my committee with their valuable knowledge and experience.

Finally and most importantly, if I did not have such a lovely family and my dear friends, I could not complete this study in an enjoyable and satisfying way.

TABLE OF CONTENTS

CHAPTERS

LIST OF FIGURES

FIGURES

CHAPTER 1

INTRODUCTION

Laser-Induced Breakdown Spectroscopy (LIBS) which may be known as Laser-Induced Plasma Spectroscopy (LIPS) or Laser Spark Spectroscopy (LSS) was used for an analytical purpose in 1963 for the first time and this was the beginning of LIBS technique. In their book, Cremers and Radziemski [1] listed some leading developments in the history of LIBS that can be seen in figure 1.1.

Laser-Induced Breakdown Spectroscopy (LIBS) is an effective atomic emission spectroscopy technique to study elemental composition of any material solid, liquid, gas or an aerosol with high precision [1,2,3,4,5]. All chemical elements can be identified by LIBS; however, the light elements ($_1$H (Hydrogen), $_2$He (Helium), $_3$Li (Lithium), $_4$Be (Beryllium), $_5$B (Boron), $_6$C (Carbon), $_7$N (Nitrogen), $_8$O (Oxygen), $_9$F (Fluorine), $_{10}$Ne (Neon), $_{11}$Na (Sodium), $_{12}$Mg (Magnesium) ...) are the best ones to be examined with LIBS due to their higher possibilities for availability in natural materials [6].

LIBS has strong connections with atomic emission spectroscopy (AES), plasma physics and laser optics. A solid state pulsed laser, focusing and collecting optics respectively for laser pulses and plasma light, a spectrometer with a fiber optic cable (FOC), a delay/pulse generator to adjust delay and gate time and a computer for data recording and system control are the fundamental components of LIBS set-up.

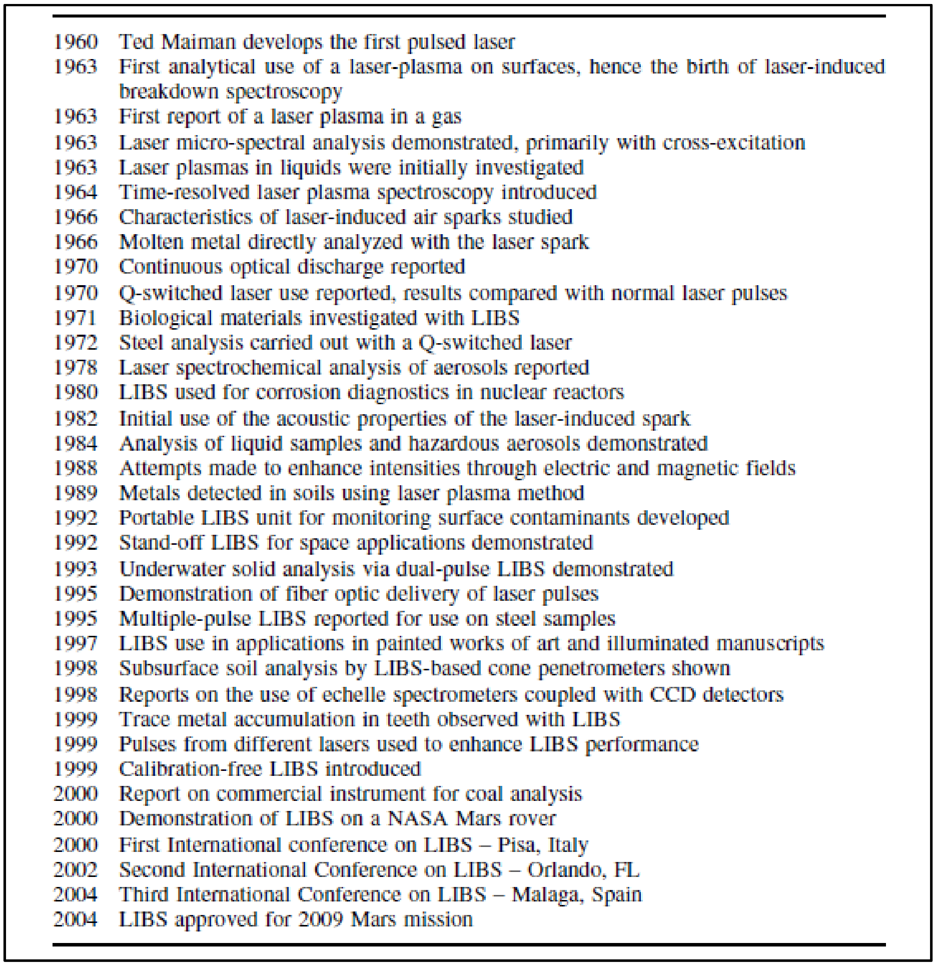

1960	Ted Maiman develops the first pulsed laser
1963	First analytical use of a laser-plasma on surfaces, hence the birth of laser-induced breakdown spectroscopy
1963	First report of a laser plasma in a gas
1963	Laser micro-spectral analysis demonstrated, primarily with cross-excitation
1963	Laser plasmas in liquids were initially investigated
1964	Time-resolved laser plasma spectroscopy introduced
1966	Characteristics of laser-induced air sparks studied
1966	Molten metal directly analyzed with the laser spark
1970	Continuous optical discharge reported
1970	Q-switched laser use reported, results compared with normal laser pulses
1971	Biological materials investigated with LIBS
1972	Steel analysis carried out with a Q-switched laser
1978	Laser spectrochemical analysis of aerosols reported
1980	LIBS used for corrosion diagnostics in nuclear reactors
1982	Initial use of the acoustic properties of the laser-induced spark
1984	Analysis of liquid samples and hazardous aerosols demonstrated
1988	Attempts made to enhance intensities through electric and magnetic fields
1989	Metals detected in soils using laser plasma method
1992	Portable LIBS unit for monitoring surface contaminants developed
1992	Stand-off LIBS for space applications demonstrated
1993	Underwater solid analysis via dual-pulse LIBS demonstrated
1995	Demonstration of fiber optic delivery of laser pulses
1995	Multiple-pulse LIBS reported for use on steel samples
1997	LIBS use in applications in painted works of art and illuminated manuscripts
1998	Subsurface soil analysis by LIBS-based cone penetrometers shown
1998	Reports on the use of echelle spectrometers coupled with CCD detectors
1999	Trace metal accumulation in teeth observed with LIBS
1999	Pulses from different lasers used to enhance LIBS performance
1999	Calibration-free LIBS introduced
2000	Report on commercial instrument for coal analysis
2000	Demonstration of LIBS on a NASA Mars rover
2000	First International conference on LIBS – Pisa, Italy
2002	Second International Conference on LIBS – Orlando, FL
2004	Third International Conference on LIBS – Malaga, Spain
2004	LIBS approved for 2009 Mars mission

Figure 1.1 The leading developments in the history of LIBS [1]

Basically, with the help of a laser source plasma is created on a material and atomic emission lines of elements existing in the plasma light are analyzed to determine the elemental characterization of the material. The main factor during the plasma formation is the laser ablation process. Focused laser light ablates the surface of the material. As a result of this interaction, the plasma formation begins and the emission spectrum occurs.

In order to understand the emphasis of plasma creation for an elemental characterization of a material, one should notice two significant processes: first, the excitation process a transition from ground state to excited state due to the absorbtion of the laser beam, and secondly, the emission of a photon taking place while electron’s return to ground state. In LIBS spectrum, the wavelength (nm) is presented in the x-axis and the y-axis shows the intensity (a.u.). In data analysis, generally, relative peak intensity or area under peak of the detected atomic or ionic line is presented in the y-axis [4]. If the spectrum is not well formed enough with its peaks or areas then the experiment must be repeated several times.

Data analysis is the final and most critical part of the LIBS process. Analytical and statistical measurement tools are used in great deal for the data analysis. After receiving many data from a material, one should analyze them step by step both in a qualitative and quantitative way since whole aim of an experiment depends on this. A qualitative analysis shows the identity of the elements in a sample. On the other hand, quantitative analysis presents the amount of each constituent in a sample with mathematical results [7]. Moreover, statistical tools are known as mathematical processes applied to a data set of a measurement. The important figures of merit for a LIBS analysis are mainly standart deviation (SD), signal-to-noise ratio (S/N) and limit-of-detection (LOD). After this, calibration curves are needed to be drawn according to concentration of each constituent found from known composition and as mentioned above peak intensity or area under peak. In this calibration curves, one should see linear fitting for a graph of each element that demonstrates conformity in an experiment. In a quantitative analysis, problems can occurr due to matrix effects causing poor data points being a reason for calibration curves that cannot be fitted linearly or in a desired way [8]. In the study [9], LIBS was applied to ancient marbles by Lazic *et al.*, examples of calibration curves were presented and mostly they (Ca, Al, Mn, Ti, Ba and Cu) were fitted linearly with straight lines; however, some of them (Si and Mg) had to be fitted nonlinearly due to their nonlinear data points. One can think that the longest part of a LIBS experiment is the data analysis part because the more you analyze, the better your result is. El Haddad *et al.* [10], emphasized that the crucial point in presenting LIBS results is giving most of the relevant information that one can search and find. For example, one should show the method of calculating the important figures of merit associated with the LIBS results which can be a good guidance for readers in this manner.

At this point, in order to understand and realize the importance of LIBS better, it will be helpful to illustrate studies accomplished with LIBS. Thakur and Singh explained in their book [2] some leading applications. One of them is a field-portable LIBS system to solve the problems arising from criminal and terrorist circumstances in society with the help of an efficient detection and identification ability of LIBS technique. Another example is a LIBS system for a single particle analysis to detect aerosols in the air that threatens both human health and environment. Furthermore, the paper by Rehse *et al.* [11] stated that rapid measurement and precise identification properties of LIBS can be used in biomedical samples such as human tissues. In their book, Cremers and Radziemski [1] presented a groundbreaking application established in 2002 by NASA Ames Research Center for planetary discovery on Mars. Figure 1.2 shows the rover having LIBS system standing on its head. In the same aim that is the detection and analysis of Mars ground such as rocks on the ground, NASA Jet Propulsion Laboratory (JPL) constructed Mars Curiosity Rover having advanced LIBS system [12] on its head displayed again in figure 1.2 and sent the rover to Mars in 2012 [13]. Today, Curiosity still continues to analyze Mars ground and sends its measurements to the scientists in NASA JPL. LIBS was used by Vadillo and Laserna [14] for the first time for analysis of geological materials which are four geological samples vanadinite, pyrite, garnet and a type of quartz (compostela's quartz) and they detected spectral lines of Mg, Mn, Fe and Si by using a solid state Nd:YAG laser operating at 532 nm.

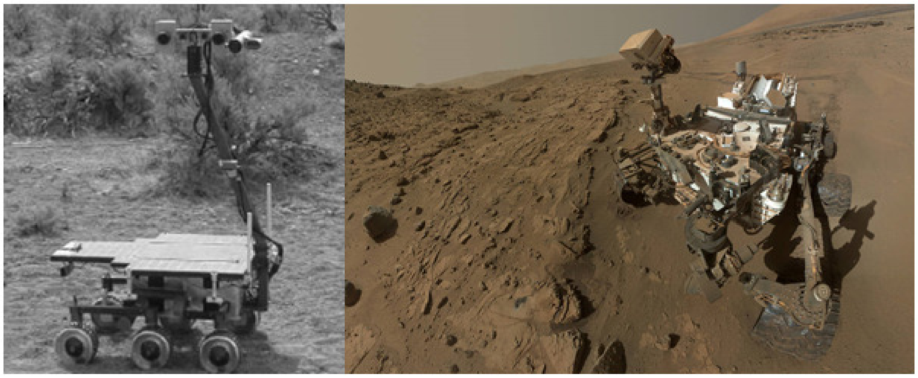

Figure 1.2 The K9 Rover (2002) [1] *left* and The Mars Curiosity Rover (2012) [13] *right*

Studies show that LIBS has a considerably wide range of applications. Moreover, several disciplines use it to enhance their studies to get better results. Among many properties of LIBS some of them may be more significant such that it requires no sample preparation, is a minimally destructive technique, provides rapid measurement and also provides the opportunity of utilization for both laboratory and field experiments. LIBS has many advantages like laser based spectroscopy techniques such as Raman Spectroscopy and Laser-Induced Fluorescence (LIF). Besides, LIBS can be combined with these methods. In the paper by Spizzichino and Fantoni [15], there is an example of such a combination property of LIBS that it is stated that for archaeological materials both Laser-Induced Fluorescence (LIF) and Laser Raman Spectroscopy show similarities in their experimental parameters and laboratory backgrounds compared with LIBS. Moreover, a stand-off sensor system gathering not only Raman but also LIBS spectra of minerals was given as another example for combination of these two techniques in the paper by Sharma *et al.* [16]. On the other hand, LIBS may have some disadvantages. For example, producing inefficient plasma signal and obtaining high LOD values due to the experimental set-up or the elements studied to be found in the samples can be pointed out as the limitations of LIBS method.

In this study, some archaeological samples are analyzed with LIBS technique. An archaeological material should be analyzed very carefully since they have several differences in structure such as surface properties which can be flat or in contrast rough. Flat surfaces are always preferable due to gaining advantages about the plasma created on materials. However, rough surfaces make measurements difficult because in that way the signal of plasma information is disturbed. Therefore, received data sets give low S/N values and high LOD values which are the main reasons for poor and unproductive qualitative and quantitative analyses. In addition, working on rare and precious materials needs to be cared during an experiment because of their fragile structures. In this point, it must be stated that the minimal destructiveness of LIBS can overcome this problem.

The archaeological rock samples of this study were selected from the samples studied in the PhD thesis "Characterization Of Emecik Limestone Figurines For Provenance" by Üftade Muşkara [17]. There are three locations excavated for sampling in Turkey. The two samples labeled as Figurine4 and Figurine22 came from Emecik, another nine samples AKYA4, AKYB(6,7), AKYC(3,4,6), KRC(1,6) and RZG2 were obtained from Datça Peninsula and K1 from Cyprus Erdemli quarry and K2 from Cyprus Değirmenlik quarry are the names of the last two samples. Totally thirteen archaeological samples dated to 6th century BC were analyzed qualitatively and quantitatively with LIBS method to obtain the elemental characterization with the help of the concentration values of each constituent existing in the results of the PhD thesis of Üftade Muşkara [17].

This thesis consists of five chapters. In chapter 1, introduction of this study is given. In the introduction part, one can find the explanation of LIBS method and related example studies. In addition, in this chapter, what the archaeological samples are and where they were excavated are introduced.

In chapter 2, theoretical background of LIBS is explained in detail. In this part, the role of laser in LIBS and the concept of laser ablation and LIBS plasma are expressed. At the end of this chapter, the emission spectrum data analysis is handled with its qualitative and quantitative parts.

In chapter 3, experimental background of this study is presented. In this chapter, the LIBS set-up is demonstrated and its components are shown and explained with their special features. In addition, the power stability of the laser and the LIBS measurement of the reference sample whose results determine the parameters of the LIBS experiments of the archaeological samples are given in this chapter. At the end of this chapter, the LIBS spectra of the archaeological samples are shown.

In chapter 4, results and discussions are given by the help of the results of the qualitative and quantitative analyses of the LIBS spectra of the archaeological samples.

In chapter 5, conclusions of this thesis are given. In this chapter, the results of this study are listed and which applications can be the future work for us is presented.

CHAPTER 2

THEORETICAL BACKGROUND

2.1 Laser In LIBS

2.1.1 Laser fundamentals

A laser source has a great role by making LIBS technique versatile. Laser light with its characteristic of high spatial and also temporal coherence differs from other light sources. When high spatial coherence is concerned, one can think that the laser beam is collimated over a wide interval. In addition, with this directionality the laser source makes working on long distance experiments of LIBS easy and comfortable like laboratory studies. Moreover, interaction of the laser light with a surface of a material brings about a concept of intensity (power per solid angle) known as irradiance because the material is irradiated by the laser light. During power calculations there is a difference between average power per area (W/cm^2) and pulsed power per area or in other name fluence (J/cm^2) [18] which is the one that will be used in the power measurements for this study. The average intensity of focused laser pulse is given below:

$$\frac{\pi E_L D^2}{4\tau_L \cdot f^2 \cdot \lambda^2 \cdot M^4}$$

where E_L = laser pulse energy, D = diameter of focusing lens, τ_L = pulse duration, f = focal length of focusing lens, λ = wavelength of laser and M^2 = beam quality [4]. Monochromaticity is another significant property of the laser beam. Unlike other light sources, a laser source can emit a narrow range of wavelengths due to the transitions in the laser medium. Therefore, it can be stated without doubt that the most significant features of the laser light are being highly coherent, collimated and monochromatic light.

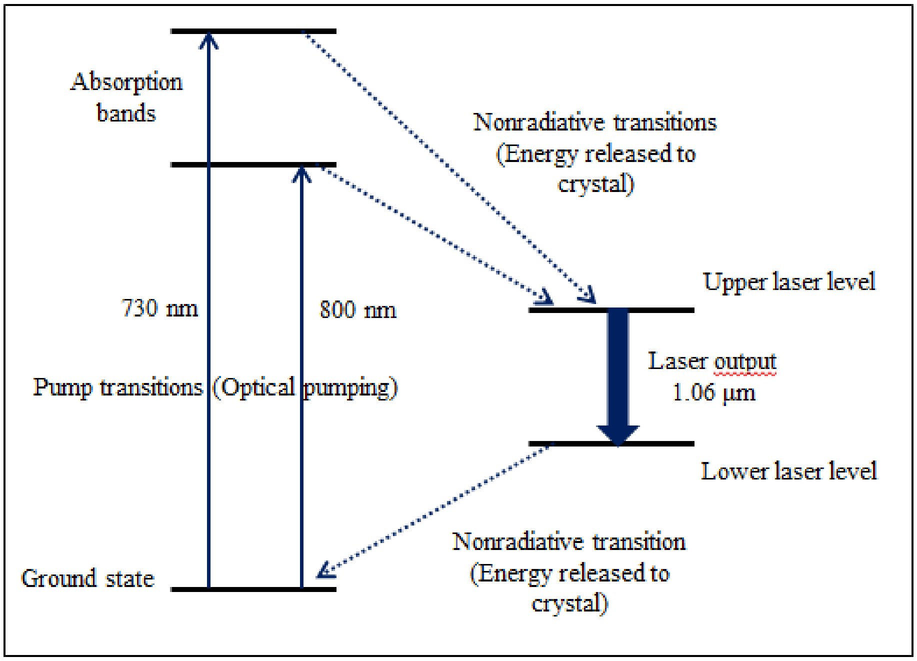

Figure 2.1 Energy levels of a Nd:YAG laser [19]

By a majority, in the LIBS experiments, solid state lasers are used and the most preferred one is Nd:YAG laser. In laser operation, high gain and low threshold can be achieved by the cubic shape of the host YAG supplying a narrow fluorescent linewidth [20]. The Nd:YAG laser operating at a wavelength of 1064 nm is formed as a result of a doped yttrium-aluminium-garnet ($Y_3Al_5O_{12}$) with (%1) triply positively charged neodymium-ions (Nd^{+3}). In this process the excitation is leaded electronically by a pump source and during the decay the amplification in a linear resonator is leaded by Q-switch [18].

In the figure 2.1, there are energy levels of a Nd:YAG laser having laser output 1.06 μm in the near-infrared region. A resonant laser cavity has the quality factor Q waiting to be modulated by the Q-switch and this modulation creates pulses which are Q-switched pulses having a pulse duration. If an output-mirror reflectivity is R and a cavity length distance between the mirrors is L in a laser medium, c/n, this pulse duration for a round trip carried out by the laser light in the laser cavity is $\frac{2Ln}{c(1-R)}$ [19]. The ratio of the stored energy in the cavity to the energy loss per round trip is known as the quality factor Q and thus if the quality factor increases, the energy loss decreases [20]. In his paper [21], Fan stated that in order to get higher efficiency (10%) and longer lifetime (20000 hr), one can use diode-pumped solid state lasers (DPSSL) instead of flashlamp-pumped lasers.

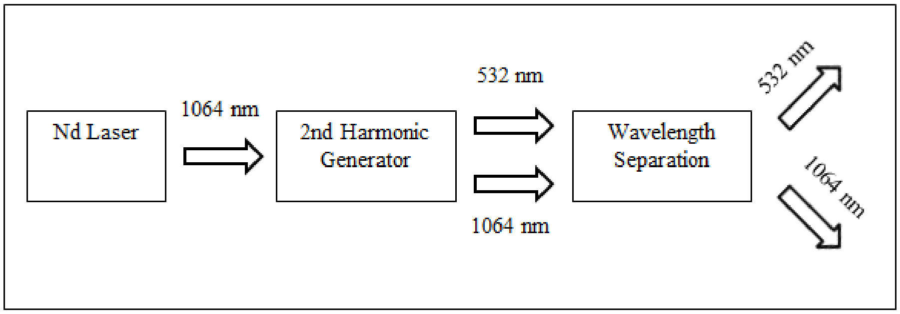

Figure 2.2 Second harmonic generation by frequency doubling [19]

Harmonic generation enables using the second harmonic (532 nm) of the primary wave (1064 nm) that means the second harmonic wave has half the wavelength of the primary wave or in other words twice the frequency and also the energy of the primary wave. Figure 2.2 shows the frequency doubling to illustrate the second harmonic generation. At the end of this process, one can use a filter to choose the 532 nm only by eliminating the 1064 nm.

2.1.2 Optical systems for LIBS set-up

Focusing laser pulses onto a material and plasma information collection are the main requirements for LIBS set-up. A simple lens can be used to focus the laser beam on a material and also a mirror can be utilized in this configuration. As a result, the lens-to-sample or lens-to-mirror-to-sample focusing system can be applied to the laser beam. After focusing the laser beam, plasma spark is created and to collect the plasma information from it one or more lenses can be used by sending the plasma light to the detection system which is a spectrometer generally. A fiber optic cable (FOC) whose one end attached to the spectrometer can be used to collect the plasma light that is focused to the other end of the FOC by the lenses. In this way, the FOC provides to gain high efficient plasma light to detect and analyze.

2.1.3 Laser ablation

Focused laser light ablates a part of a solid material due to heating, melting and vaporization processes with the help of the laser energy. The ablated mass from the surface is transformed into many species and particles. This interaction between the laser light and the material results in a formation of plasma and its emission spectrum. The critical point for LIBS is the laser ablation that is the first significant step among several steps in a LIBS experiment. The importance of no sample preparation and rapid measurement properties of LIBS comes from the laser ablation process. The laser pulse lengths determine the portion ablated and in which shape the ablation occurs. The microsecond and nanosecond pulsed lasers carry out all the processes heating, melting and vaporization. However, the femtosecond pulsed lasers which have shorter time scale than plasma light skip the first two steps and lead to direct vaporization. Figure 2.3 demonstrates this according to the lasers operating at three different types of wavelength.

Nanosecond pulsed lasers are chosen if an aim of an experiment depends on an analytical application [2] and LIBS as an analytical tool for an elemental characterization of a material is the best example for this.

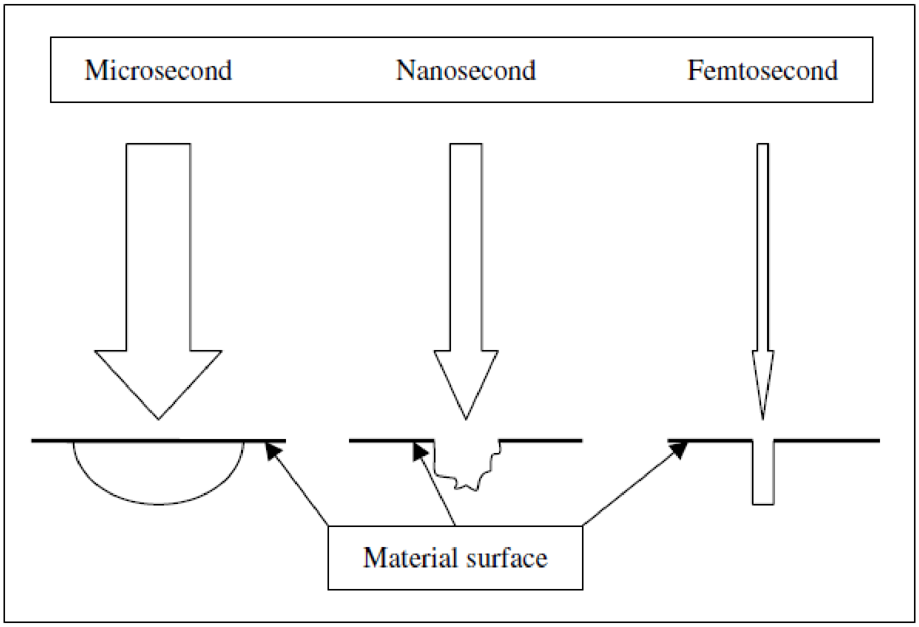

Figure 2.3 Laser ablation at different pulse lengths [1]

2.2 LIBS Plasma

2.2.1 Atomic emission spectroscopy

Atomic emission spectroscopy (AES) is used to detect and analyze the characteristics of the photons emitted by atoms or molecules. Every element has atomic or ionic spectral line at certain wavelength and intensity because of electron transitions between atomic orbitals. Absorption is defined as the transition of an electron from a lower state to a higher state due to staying under the influence of a source such as laser light. On the other hand, in the opposite situation, an electron return from a higher state to a lower state causes an emission of a photon. After the determination of the spectral lines with their wavelengths and intensities by making inferences about which transition belongs to which spectral line, the presence of related elements in a material can be revealed.

2.2.2 Radiations from plasma

Plasma is the fourth state of matter. Plasmas consist of negatively charged particles that are free electrons stripped away from their orbitals around a nucleus and positively charged particles that are ions moving freely. These charged particles cause plasmas to interact with electric and magnetic fields in an intense way.

If the ratio of electrons to other species such as atoms and ions is less than 10% in a plasma, it is called a weakly ionized plasma which characterizes LIBS plasma generally [1]. Plasma radiation process contains continuum emissions, ionizations and line emissions.

Free-bound transition (radiative recombination) and free-free transition (Bremsstrahlung emission) are the main continuum emissions. When the sum of the kinetic energy of the free electron ($\frac{1}{2}m_e v_e^2$) and the ionization energy of the atom (ε) is higher than the energy of the bound state (E_j), this bound level captures the free electron from the free state by an ion. As a result of this free-bound transition or in other name radiative recombination, a photon with the photon energy hv is emitted. On the other hand, a decelerated electron in a collision or an interaction with an ion causes an emission of photon due to the loss of kinetic energy of the electron that is the reason of free-free transition known as Bremsstrahlung emission. Furthermore, there can be seen bound-bound transition and also ionization from a ground state or an excited state. Figure 2.4 represents the basic transitions for an atom or ion.

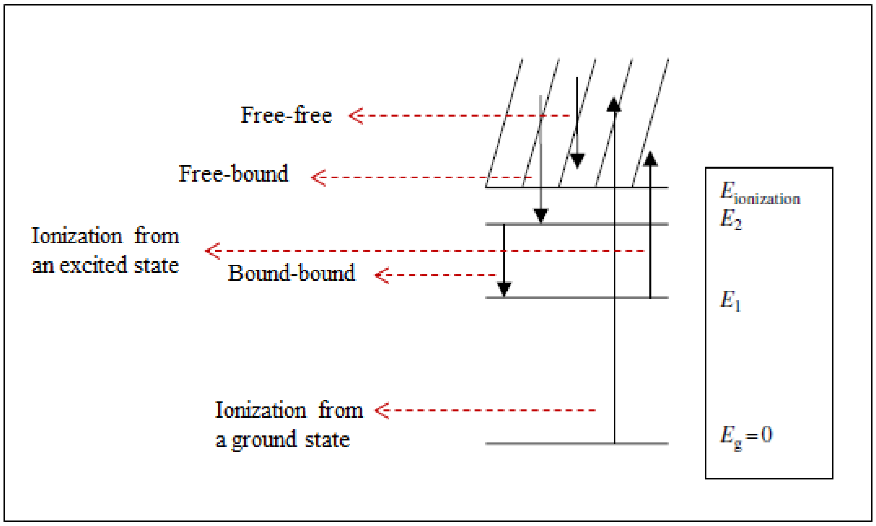

Figure 2.4 Basic transitions occurring in an atom or ion [1]

Line emissions between the energy levels E_1 and E_2 can be represented in three different types of processes spontaneous emission, stimulated (induced) emission and absorption. Einstein's A and B coefficients A_{21}, B_{21} and B_{12}, the populations of the energy levels N_1 and N_2 and external radiation of density $\rho(v_{12})$ where v_{12} is the frequency of the spectral line occuring during the transition between the energy levels are used to define both the probability of the transition and the number of the transitions for these radiations [2]. The intensity or the emissivity of the spectral line is connected with the probability of the transitions and the population of the energy levels. Figure 2.5 shows all processes with their proper definitions in terms of these parameters.

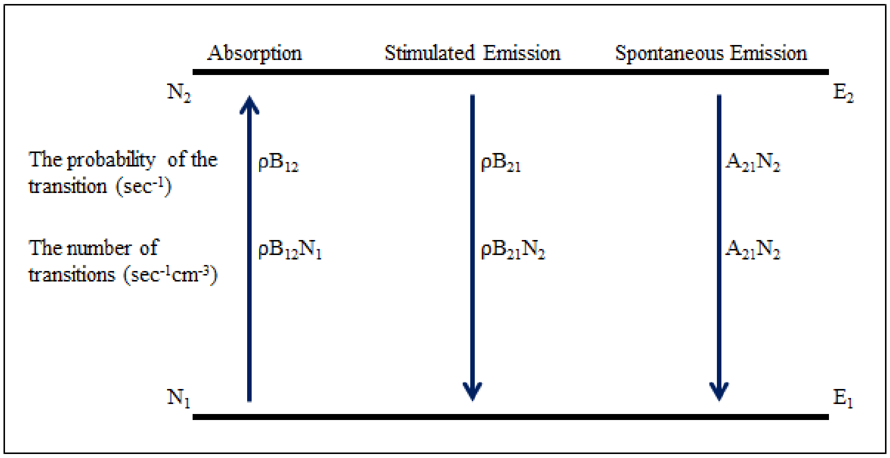

Figure 2.5 Radiations from atoms between two energy states [2]

2.2.3 Time window for LIBS plasma

When focused laser light is absorbed by a target surface, plasma is created. If plasma formation is thought as plasma cloud or plume, continuum emissions are seen near the surface, where plasma is hot and touches the surface almost, and line emissions are seen towards the end of the plasma expansion, where plasma is cold [2]. However, these processes occur in very short time. Generally, the delay time (t_d) is set in nanosecond(ns) time scale and the gate pulse width (t_b) is set in microsecond(μs) time scale. The time between the plasma formation and the moment of the observation of the plasma spark is t_d and the recording time of the plasma light is t_b [4]. Plasma lifetime is roughly in the range of 300 ns and 40 μs [22]. Therefore, for an accurate elemental analysis, one should arrange the delay time and gate width according to their convenient time regimes to record the emission correctly. This time window is vital for observation of plasma because continuum emissions generating noise in the spectrum can be thought as background of line emissions which leads to poor line emissions and thus bad signal-to-noise ratio (S/N). One of the important figures of merit for an analysis of LIBS measurements is S/N. S/N indicates how well an experiment is performed that is the sign of the precision of the measurements. In the spectrum, line emissions are the important radiations for the elemental analysis of the target and hence experiments are performed in order to be able to gain less background or noise and high intensity for lines at the same time.

2.3 Emission Spectrum Data Analysis

2.3.1 Qualitative analysis

Determination of elements in a material or in other words telling which elements exist in a material with the analysis of the plasma information that gives the spectral emissions of the elements in terms of the wavelengths and intensities generates qualitative analysis.

There is an important concept about persistent lines of an element that should be tried to find to make the qualitative analysis accurately. During the excitation process of a specific element, in order to find the persistent lines of that element which is low concentrated with respect to other substances in an arc or discharge source, one should reduce the concentration to see the decrease in the number of observable lines of that element until the persistent or sensitive lines continue to exist [23]. If the emission spectrum consists of these persistent lines, inherently one can say that this element exists qualitatively in the material measured with LIBS.

There are persistent lines of first ionization like Mg (I) or Cr (I) and second ionization as Mg (II) or Cr (II) that are the examples encountered in LIBS emission spectrum. Meggers presented both of them in his papers [24,25] that one can find the characteristics of the persistent lines of many elements. Moreover, The National Institute of Standards and Technology (NIST) offers more comprehensive lists about these persistent lines under the title of National Standard Reference Data Series (NSRDS) which were the studies of Moore [26]. These private and public database collections are not the only ones, because many people and organizations are working for contribution to these databases that helps them grow rapidly day after day.

2.3.2 Quantitative analysis

After obtaining the elements existing in a material, the next step is to prove it with mathematical results that is the main purpose of quantitative analysis. The crucial point is setting calibration curves for the obtained elements. For illustration, in one of these graphs, as in all other graphs, x-axis needs to be the concentration of the element in a known mixture and y-axis can be the peak intensity of this element that is presented in the LIBS spectrum as the line intensity or, in the same aim, y-axis can be the area under peak of this spectral line. Generally, for a LIBS experiment, concentrations values of elements are in the range of mg/kg or ppm (10^{-6}) and intensities or areas have arbitrary unit (a.u.). An ideal calibration curve which is ordinarily difficult to obtain passes through the origin and has a low standard deviation that means the data values are in harmony diagonally and do not spread out in the graph, and thus the result is a straight line.

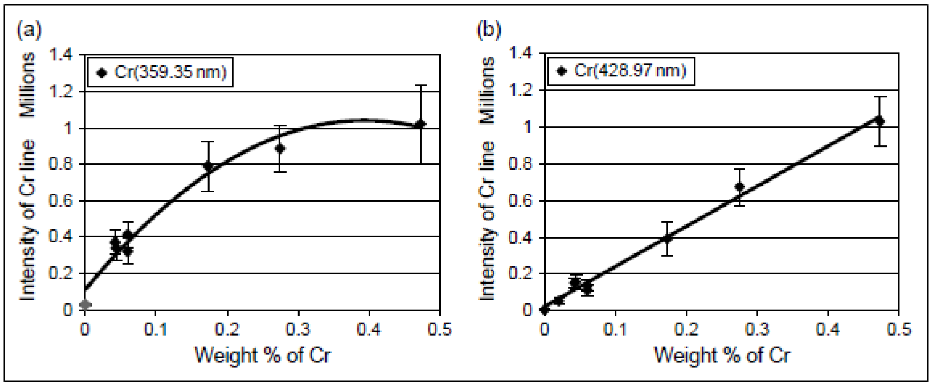

Figure 2.6 Calibration curves for Cr lines at 359.35 nm (a) and 428.97 nm (b) [2]

Figure 2.6 gives an example containing nonlinearly and linearly fitted calibration curves respectively for Cr lines at 359.35 nm and 428.97 nm. A good calibration curve can be handicapped by matrix effects limiting the performance of LIBS method. It can be a problem arising from experimental parameters of LIBS set-up or disturbed emission lines of elements in a LIBS spectrum. Matrix effects have serious influences on calibration curves. In order to overcome these obstacles one can set the value of the ratio of the peak intensity or area under peak of related element to the background of its LIBS spectrum or the appropriate element line or molecule band again from its LIBS spectrum as the y-axis in calibration curves. This procedure enhances the linearity to approach the ideal calibration curve.

CHAPTER 3

EXPERIMENTAL

3.1 LIBS Set-up

The whole LIBS set-up is seen in figures 3.1 and 3.2 from different perspectives. The alignment of the set-up is the most important and sensitive part since the plasma light should be collected on the center of the FOC precisely to see all the spectral lines of elements existing in materials. Any disturbance over the alignment can cause wrong measurement easily. Furthermore, figure 3.3 presents the schematic view of this homemade LIBS set-up.

The set-up consists of two significant paths. One path focuses the laser pulses coming from the compact pulsed Nd:YAG laser on a material and other path collects the plasma signal created on a material by the focused laser pulses. In these processes, the delay/pulse generator used to adjust delay time and gate pulse width for the laser pulses, the spectrometer utilized to get LIBS spectra and the computer used for LIBS data recording and system control are the other main components of this LIBS set-up.

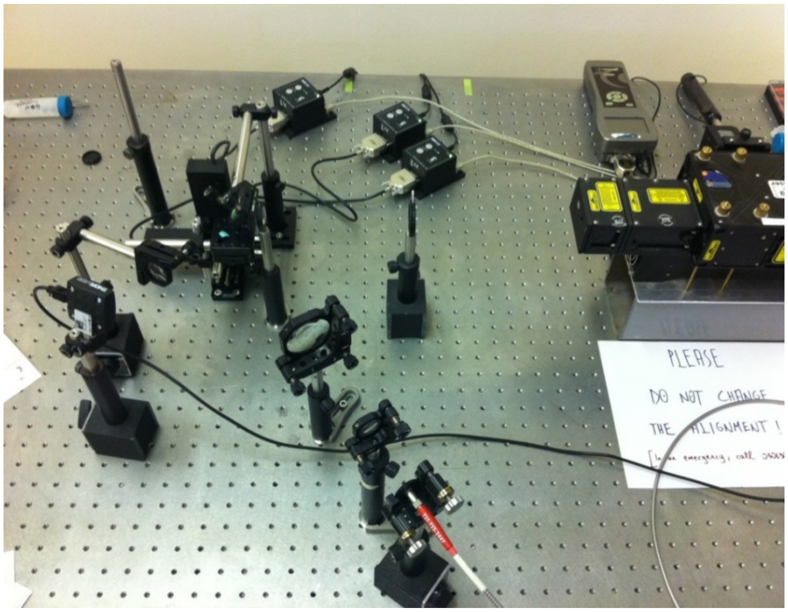

Figure 3.1 LIBS set-up view from side

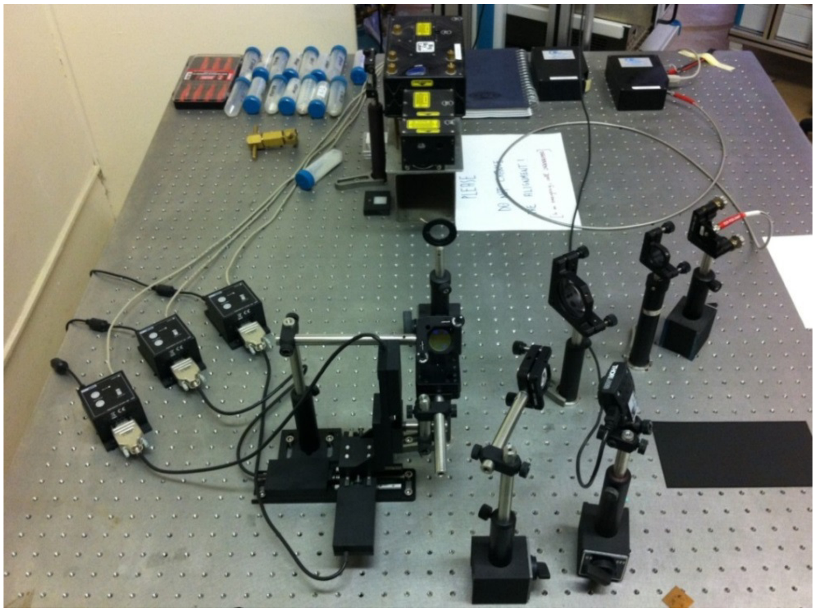

Figure 3.2 LIBS set-up view from top

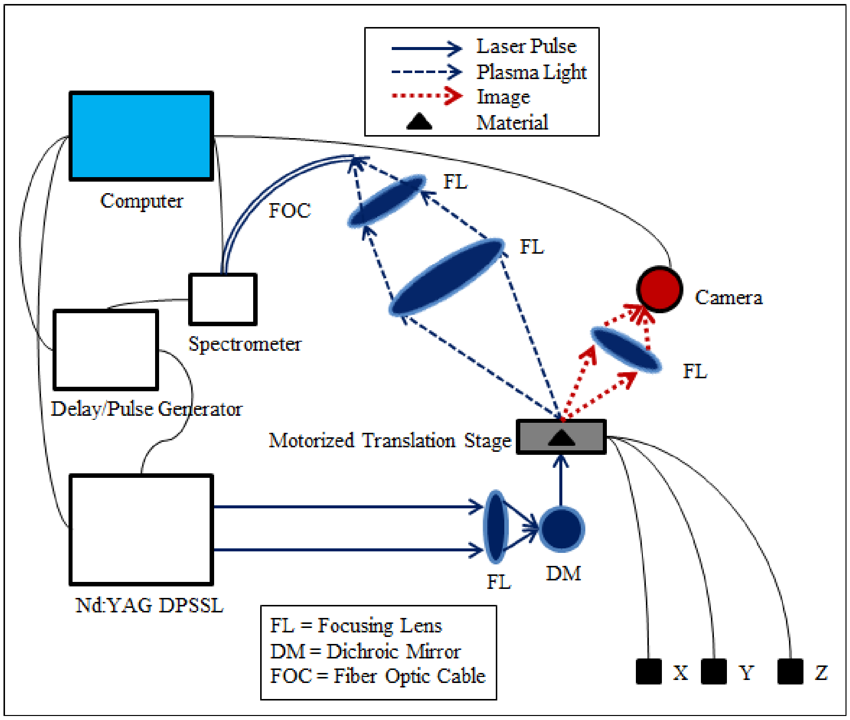

Figure 3.3 Schematic view of LIBS set-up

The first fundamental apparatus is Centurion DPSSL from Quantel used as a source to create plasma onto materials. This compact pulsed Nd:YAG laser shown in figure 3.4 operates at a wavelength of 532 nm the second harmonic of the primary wave 1064 nm. The laser has maximum 25.5 mJ pulse energy in nanosecond pulses whose durations are 8 ns approximately. Moreover, the laser has a possibility for repetition rates up to 100 Hz. The laser is fired and stopped via its computer program “Centurion Control” that is also used for setting the parameters of the laser pulse. The pulse energy is inversely proportional with the Q-switch delay where the pulse energy is adjusted on the program and the reason of this is the quality factor Q as explained in the theoretical background.

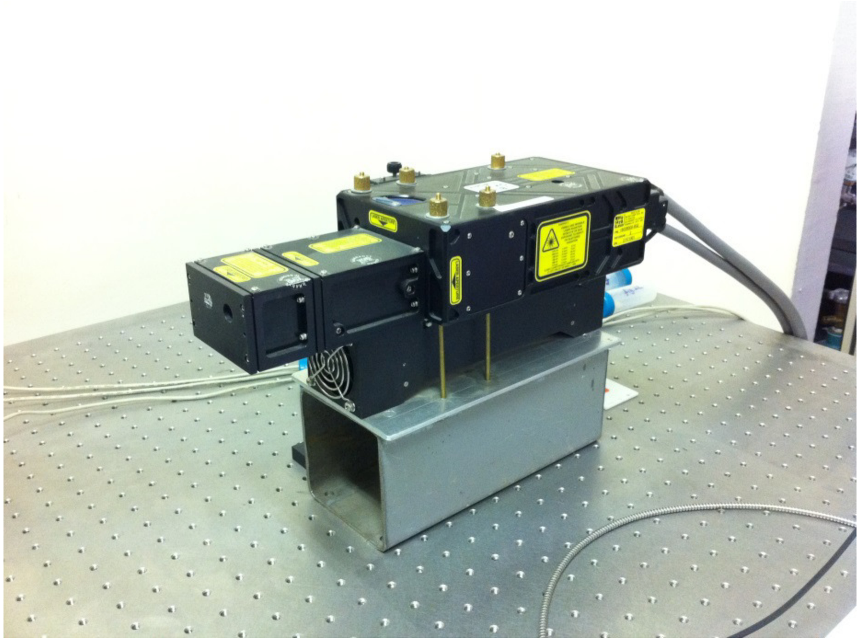

Figure 3.4 Nd:YAG DPSSL

Figure 3.5 DG535 Delay/Pulse Generator

The next one is Model DG535 Digital Delay/Pulse Generator of Stanford Research Systems which is connected with the laser and spectrometer and directly related with the laser pulse. This generator seen in figure 3.5 is utilized to adjust the delay time (t_d) the time before the initiation of each pulse and the gate pulse width (t_b) the time between the beginning and ending of each pulse. The generator performs the process by external triggering that is the crucial point for multiple shots analysis because record of every shot is important and any of them should not be missed in order to obtain an accurate LIBS spectrum and a complete data analysis. Furthermore, a labview code is made to control the generator from the computer and its front panel can be seen in figure 3.6. In the panel there are two significant parameters which are A and B representing the delay time and gate pulse width respectively.

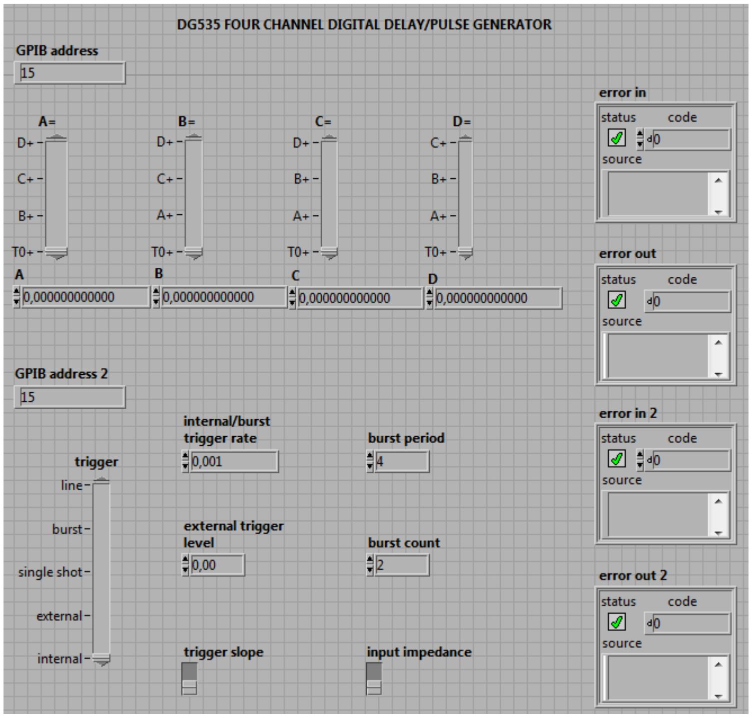
DG535 FOUR CHANNEL DIGITAL DELAY/PULSE GENERATOR

GPIB address: 15

A: 0,000000000000
B: 0,000000000000
C: 0,000000000000
D: 0,000000000000

GPIB address 2: 15

internal/burst trigger rate: 0,001
burst period: 4
external trigger level: 0,00
burst count: 2

error in: status ✓ code 0
error out: status ✓ code 0
error in 2: status ✓ code 0
error out 2: status ✓ code 0

Figure 3.6 Front panel of Labview code for
Delay/Pulse Generator

The last device is Ocean Optics HR2000+ High Resolution Spectrometer shown in figure 3.7 connected with the delay/pulse generator and also has a connection with the one end of the FOC collecting the plasma information with its other end. The spectrometer has the range of 190 - 1100 nm and minimum 0.035 nm optical resolution. The spectrometer receives the plasma information and gives the LIBS spectrum with the aid of its computer program "Ocean Optics SpectraSuit" displaying graphs of intensity vs. wavelength. Moreover, this program is used to take a record of data.

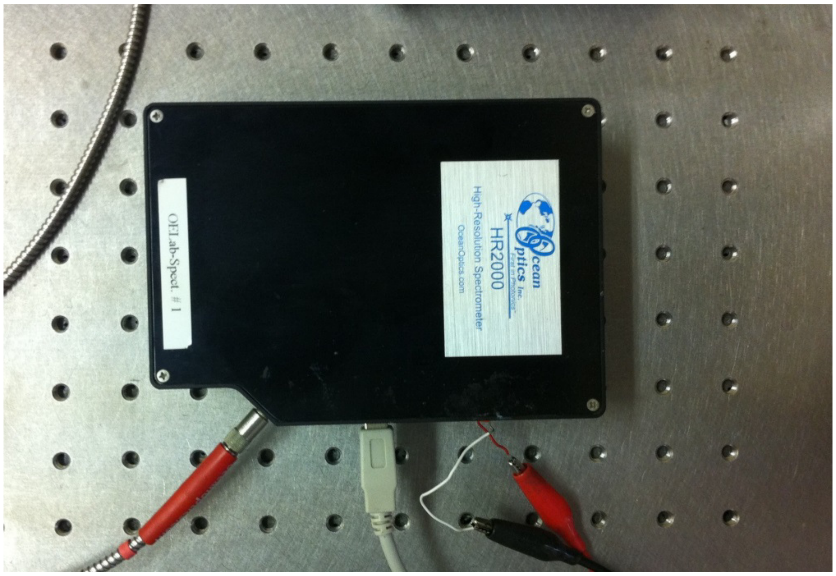

Figure 3.7 HR2000+ Spectrometer

The focusing system of the LIBS set-up consists of one focusing lens with a focal length of 5 cm interacting with the laser pulse parallel to the optical table and one dichroic mirror transmitting the wavelength of 1064 nm and reflecting the wavelength of 532 nm focused beam with a 90 degree angle downwards onto the sample standing on a 50 mm Compact Motorized XYZ Translation Stage from Thorlabs. Figure 3.8 shows the focusing part and motorized xyz translation stage closely. In addition, in order to control the translation stage from the computer the labview code is generated again. The aim is similar with building the labview code of the generator that is to achieve more compact and faster measurements. Figure 3.9 represents the front panel of this labview code. One can set distances for all directions x, y and z simultaneously to place a material to a desired location. Because of the extreme sensitivity of LIBS set-up, fine adjustments are needed for the position of the sample and the translation stage with its labview code can overcome this issue by its millimetric movement feature in each of the x, y and z directions.

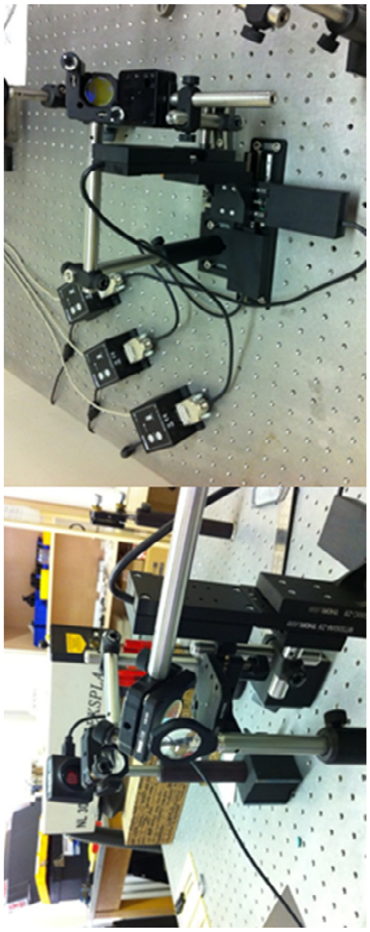

Figure 3.8 Focusing part of LIBS set-up and Compact Motorized XYZ Translation Stage

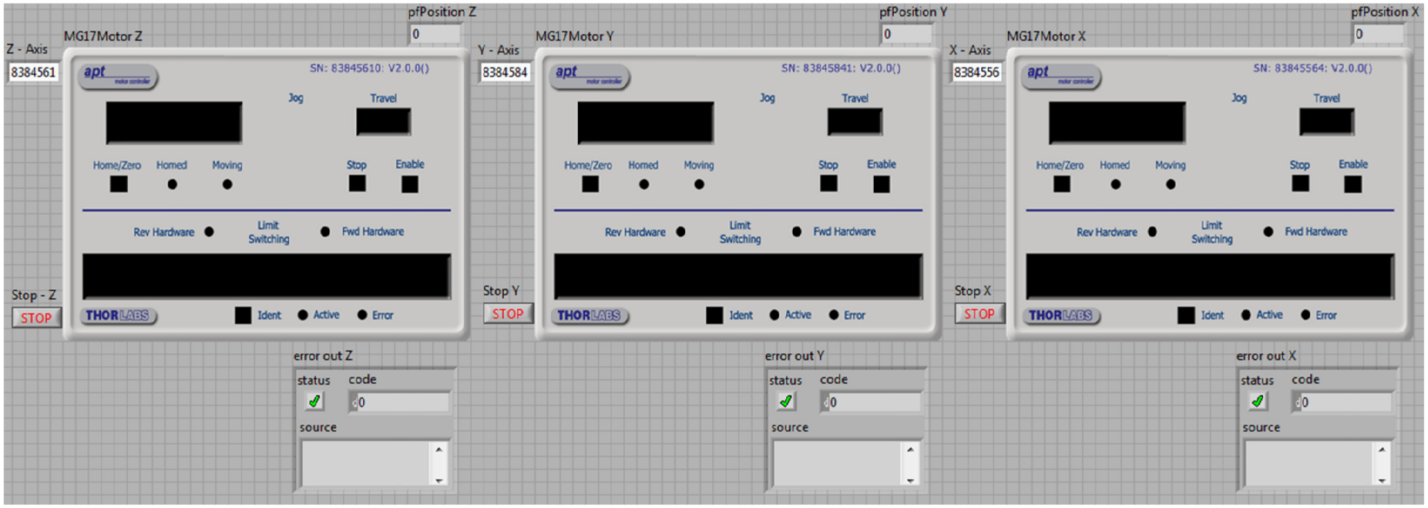

Z - Axis 8384561
pfPosition Z 0
error out Z: status ✓ code 0
Y - Axis 8384584
pfPosition Y 0
error out Y: status ✓ code 0
X - Axis 8384556
pfPosition X 0
error out X: status ✓ code 0

Figure 3.9 Front panel of Labview code for motorized xyz translation stage

Moreover, there is a camera in the LIBS set-up. In the sense of working to make the images of the materials sharp or clear on the camera, DCC1645C Compact CMOS USB 2.0 Camera of Thorlabs and one focusing lens with a focal length of 7.5 cm are used to determine the appropriate positions of x, y and z directions of the materials by using the translation stage. In other words, the more clear display constructed with the camera and lens, the better the alignment is. In this manner, the alignment of the plasma light that should be fallen onto the center of the FOC can be adjusted to get a correct LIBS spectrum. Furthermore, after every measurement, the photos of the materials are taken through the camera and one can see all the craters formed on the surfaces of the materials due to the focused laser pulse. Figure 3.10 presents the camera and focusing lens and also the different view of them can be seen in the first picture of the figure 3.8.

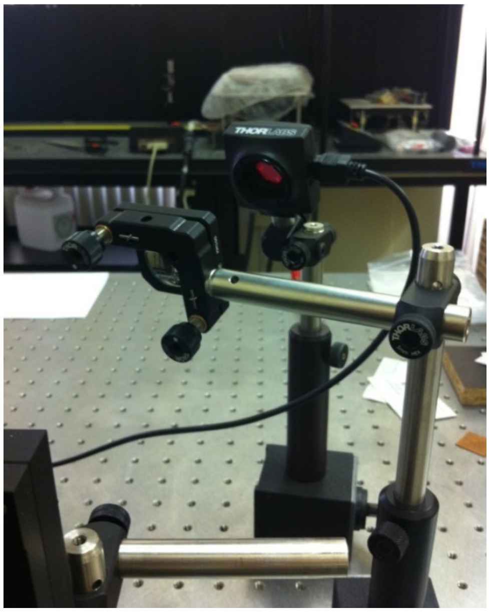

Figure 3.10 Compact CMOS USB 2.0 Camera and focusing lens

The plasma information collecting system has a succession of two lenses with focal lengths of 30 cm the first one and 10 cm the second one. These two lenses collect the plasma light and focus it to the center of the one end of the FOC whose other end is attached to the spectrometer. The logic of using firstly the lens with a higher focal length is not to lose any plasma light. Furthermore, focusing the laser pulse twice enhance the collected plasma light over the FOC. Figure 3.11 shows the close-up of the collecting part.

Figure 3.11 Collecting part of LIBS set-up

3.2 Power Measurement

At specific time intervals that can be days or months or years power measurements of a laser should be performed firstly before starting a LIBS experiment because one of the most important criteria to carry out LIBS experiments successfully is having power stability. Power stability provides consistency in measurements bringing along a good comparison among data analyses and results of several materials. As mentioned in the theoretical background, pulsed power per area or in other name fluence (J/cm^2) is measured instead of average power per area (W/cm^2) due to using the pulsed Nd:YAG laser. In order to not damage the powermeter by the laser pulse one negative lens with a focal length of 10 cm is placed between them. The set-up of power measurement is seen in figure 3.12.

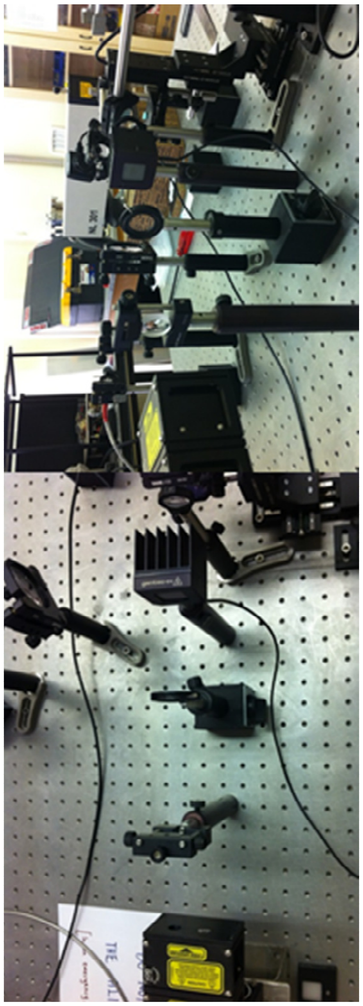

Figure 3.12 Set-up of power measurement

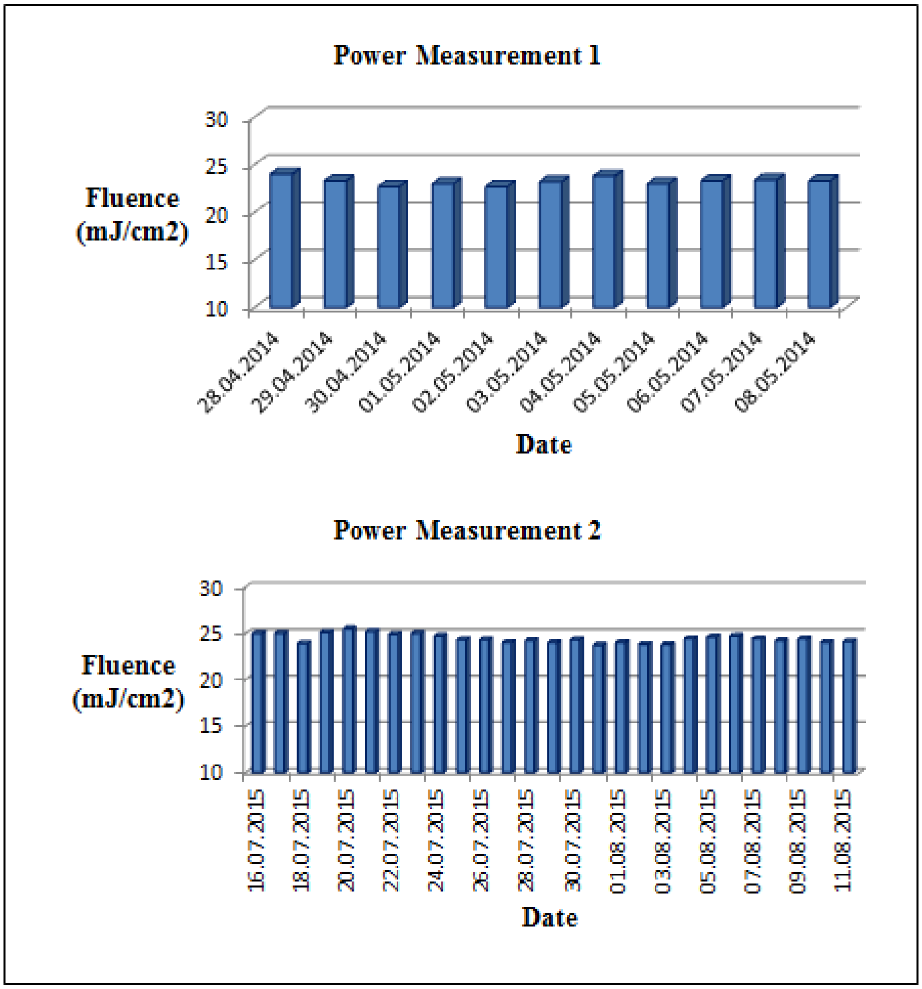

Figure 3.13 Power measurements for several time intervals

Figure 3.13 shows the power measurements for several time intervals. The result ensures that the power stability of the laser pulse exists and averagely the maximum value of the fluence is 24.1 mJ/cm^2 per pulse at 150 μs Q-switch delay when the laser pulse energy is maximum and during the measurements the frequency is always kept at 1 Hz.

3.3 LIBS Measurement of The Test Material (R291)

In this study, before the LIBS experiment of the archaeological materials, the test material (R291) again obtained from the PhD thesis [17] of Üftade Muşkara and having similar features with the archaeological samples has been analyzed as a reference in the LIBS set-up. This measurement is a preliminary work for the archeological materials whose optimum delay time and gate pulse width can be determined at the end of this experiment. The measurement is performed with many different delay times and gate pulse widths. The aim here is to choose which time window is the best for the measurement of the archeological materials by LIBS. The delay times of 100, 300, 500 and 1000 ns and gate pulse widths of 5, 10, 15 and 20 μs are applied in such a way that all pair options of them are used. Thereafter, the signal-to-noise ratios (S/Ns) at all suitable peaks for each data set are calculated. As a result, the pair of 300 ns delay time and 20 μs gate pulse width with the higher S/N values is found to be the most proper condition for the LIBS experiment of the archaeological samples. Figures 3.14 and 3.15 show the graphs of S/N vs. gate pulse width at 300 ns delay time and S/N vs. delay time at 20 μs gate pulse width, respectively.

It should be known that the aim of choosing this time window, 300 ns delay time and 20 μs gate pulse width, due to their higher S/N values is to obtain successful LIBS measurements for the archaeological samples because high S/N values means high peak intensities for the spectral lines of the detected elements.

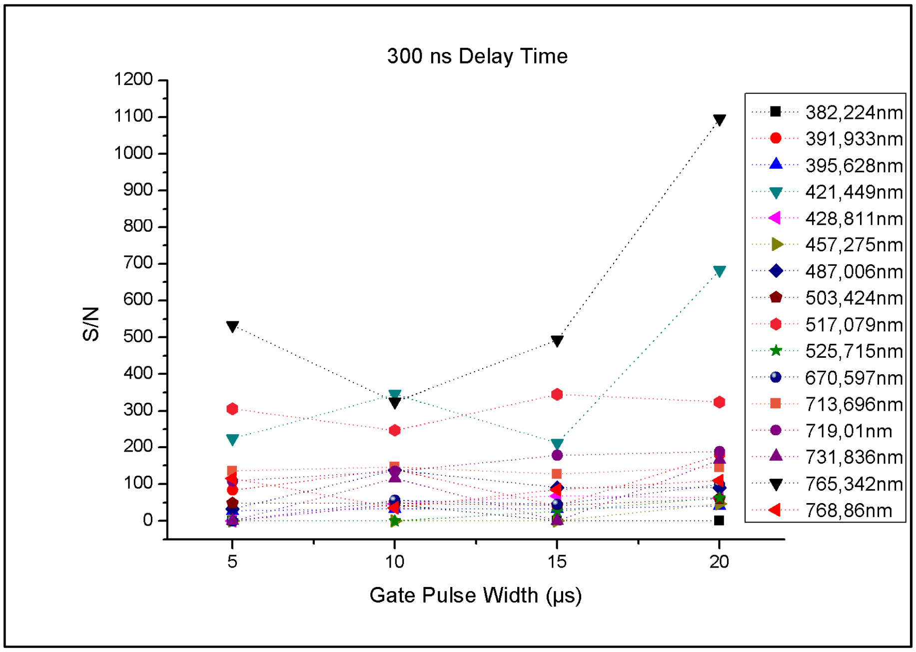

Figure 3.14 S/N for all gate pulse widths at 300 ns delay time

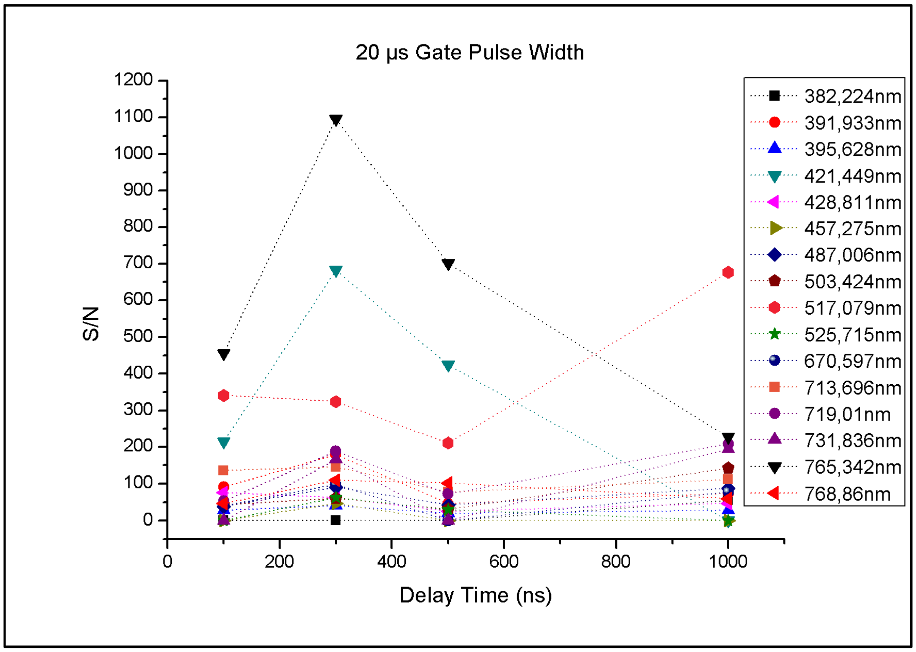

Figure 3.15 S/N for all delay times at 20 μs gate pulse width

3.4 LIBS Measurement of The Archaeological Materials

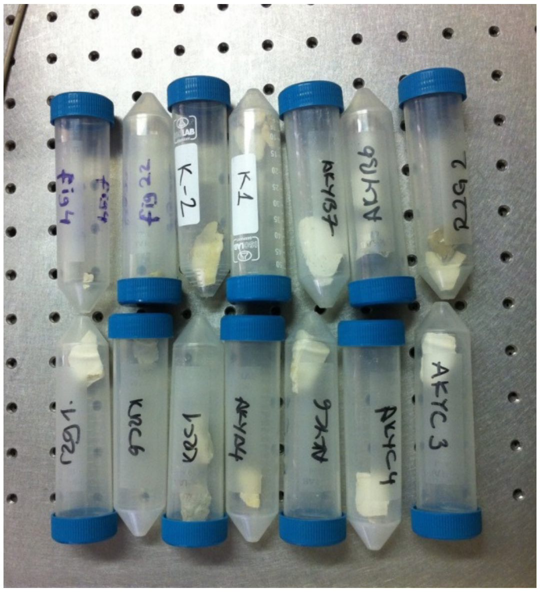

Figure 3.16 Archaeological materials

After the identification of the time window, thirteen archaeological materials whose origins are explained in the introduction and labelled as Figurine4, Figurine22, AKYA4, AKYB(6,7), AKYC(3,4,6), KRC(1,6), RZG2, K1 and K2, seen in figure 3.16 with their protection tubes, are studied in the LIBS set-up. The parameters of the laser pulse during the experiments are sorted below. These thirteen materials are measured under the same parameters in the LIBS set-up.

- Wavelength: 532 nm
- Pulse duration: 8 ns
- Frequency: 1 Hz
- Q-switch delay: 150 μs
- Fluence: 24.1 mJ/cm^2

- External triggering
- Delay time: 300 ns
- Gate pulse width: 20 μs
- Laser shots: 5 x 30

The last parameter about the laser shots states that for each of the five different locations on the surface of any material there are thirty shots that are focused laser pulses.

After collecting the plasma light created on the surface of the material by the focused laser pulse, the LIBS spectrum is obtained in the form of the graph of intensity (a.u.) vs. wavelength (nm) through the spectrometer and computer. All the LIBS spectra of the materials including labeling the common peaks whose S/Ns can be calculated without any problems are shown in figures 3.17-29. In these figures, there are photos of the archaeological samples taken by both the normal camera and the camera of the LIBS set-up. It is understood from the pictures that there are micrometric or milimetric craters formed on the surfaces due to the focused laser pulses.

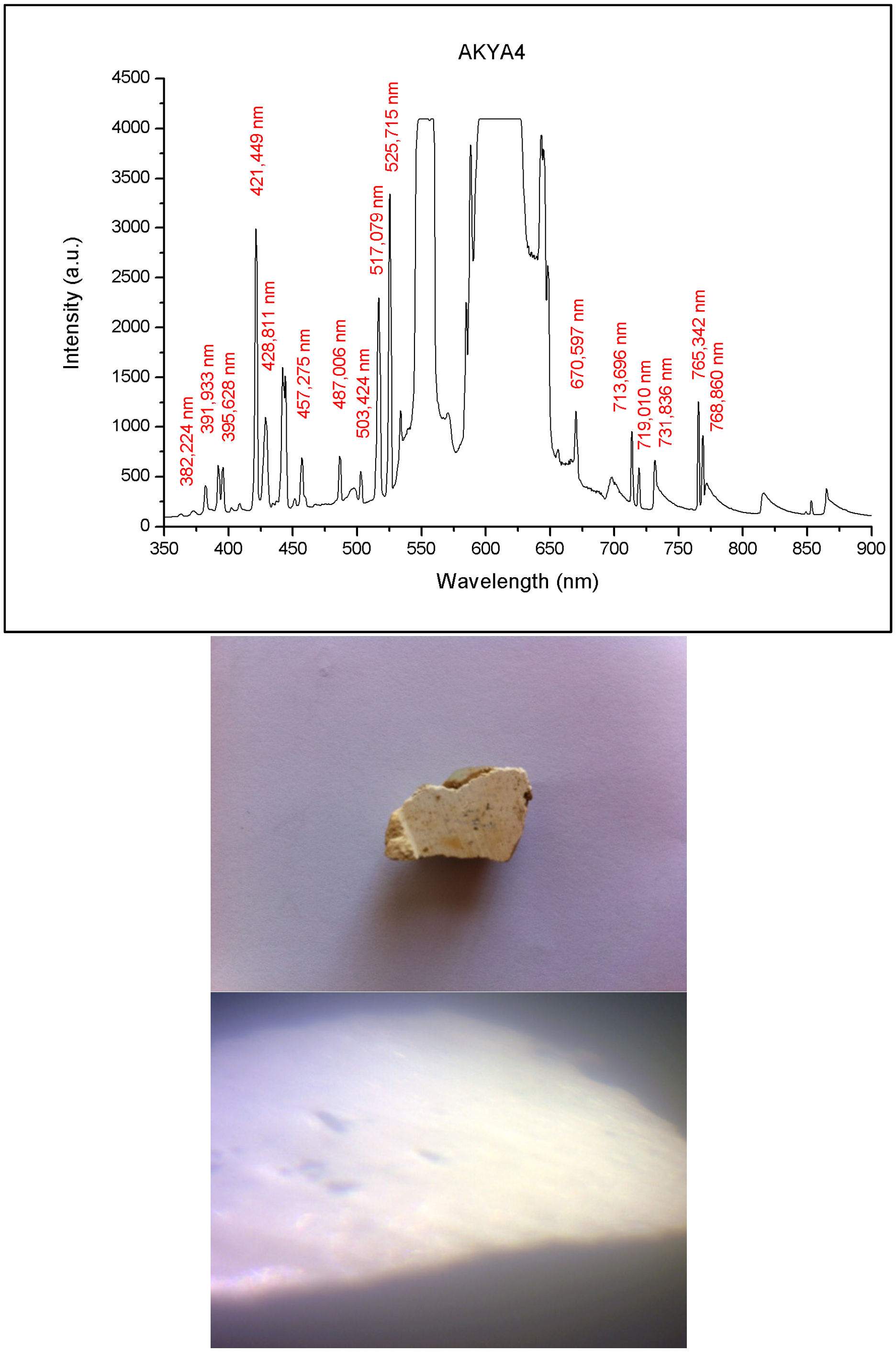

Figure 3.17 LIBS spectrum and photos of AKYA4

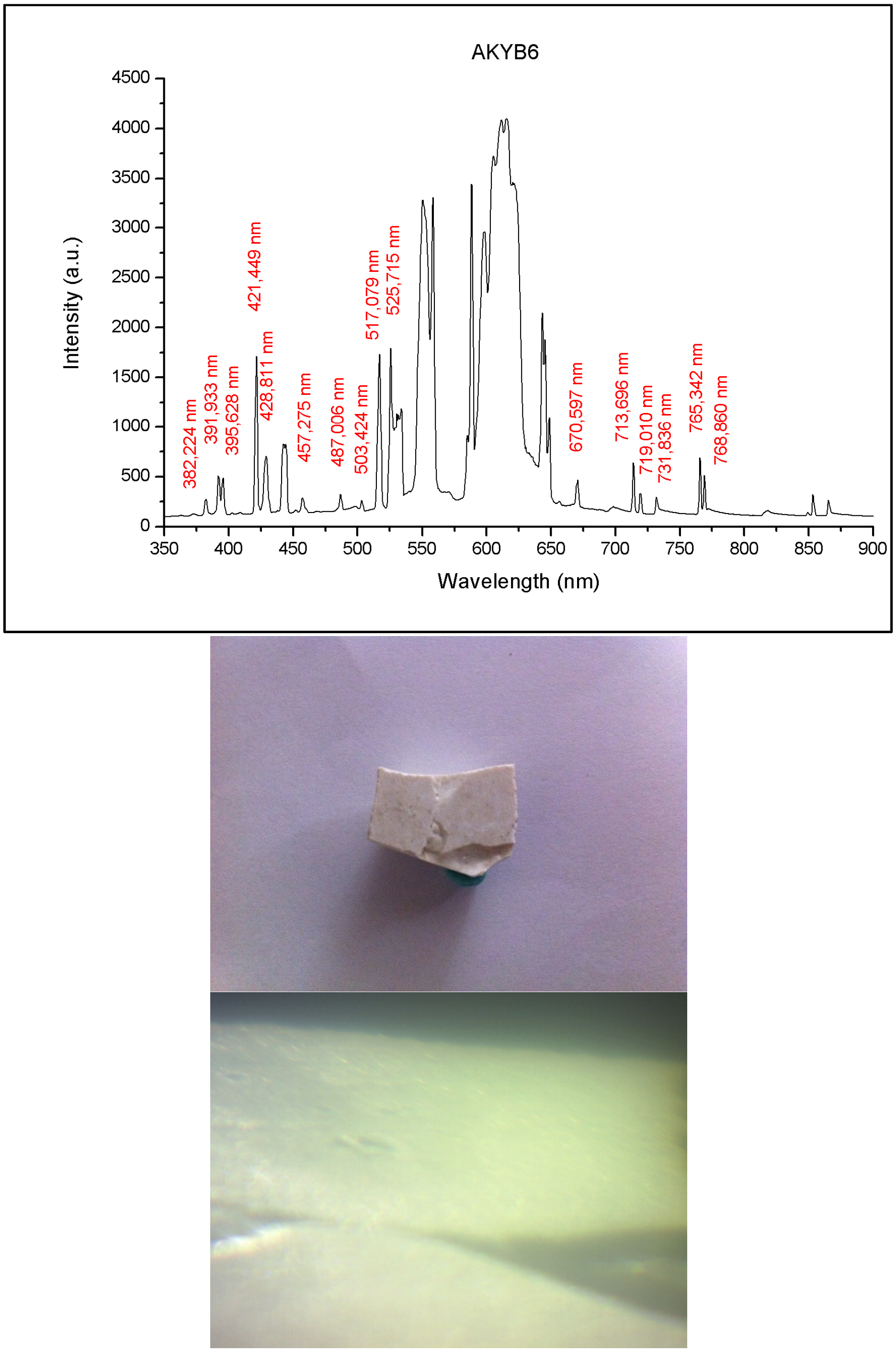

Figure 3.18 LIBS spectrum and photos of AKYB6

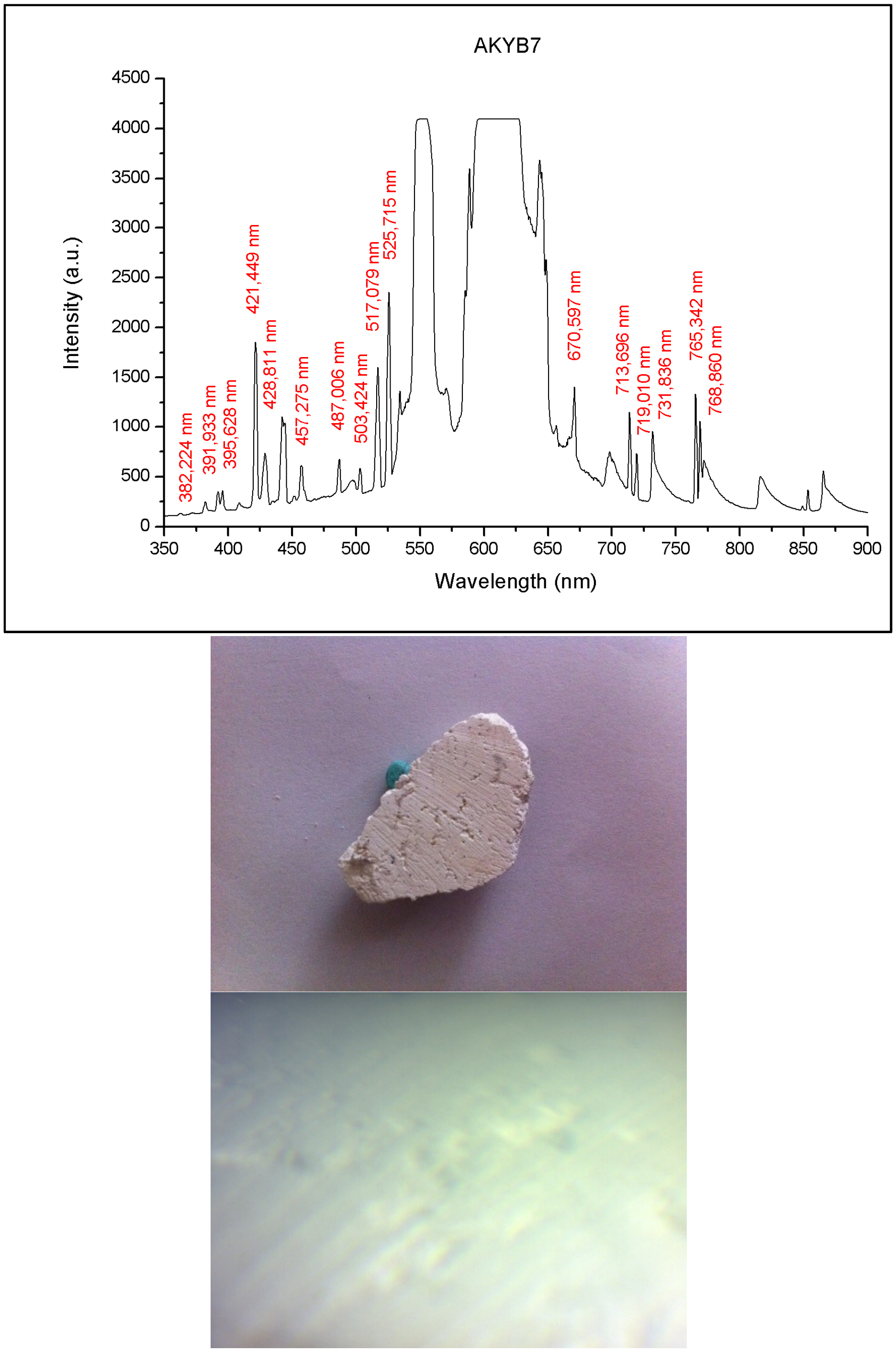

Figure 3.19 LIBS spectrum and photos of AKYB7

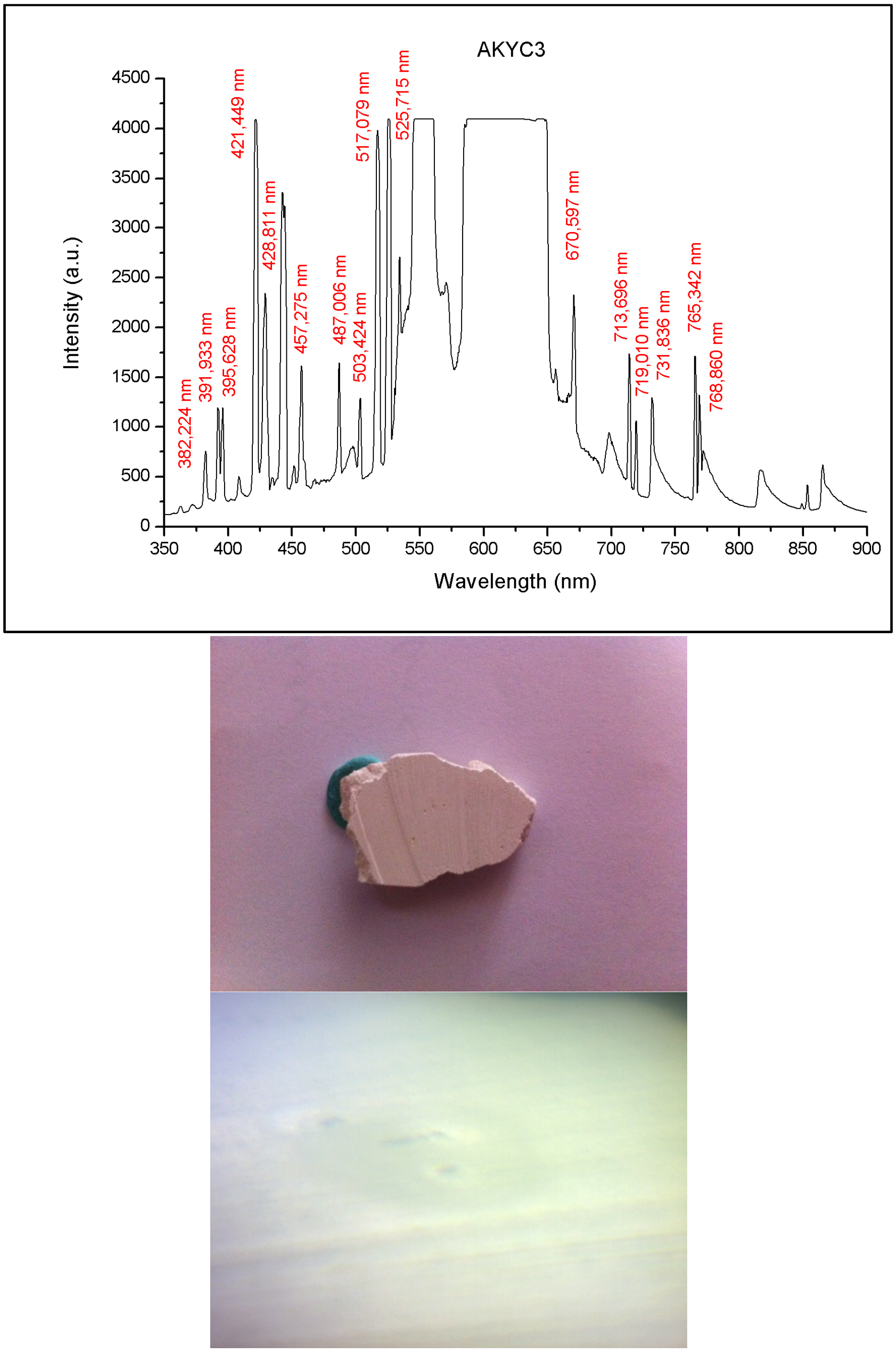

Figure 3.20 LIBS spectrum and photos of AKYC3

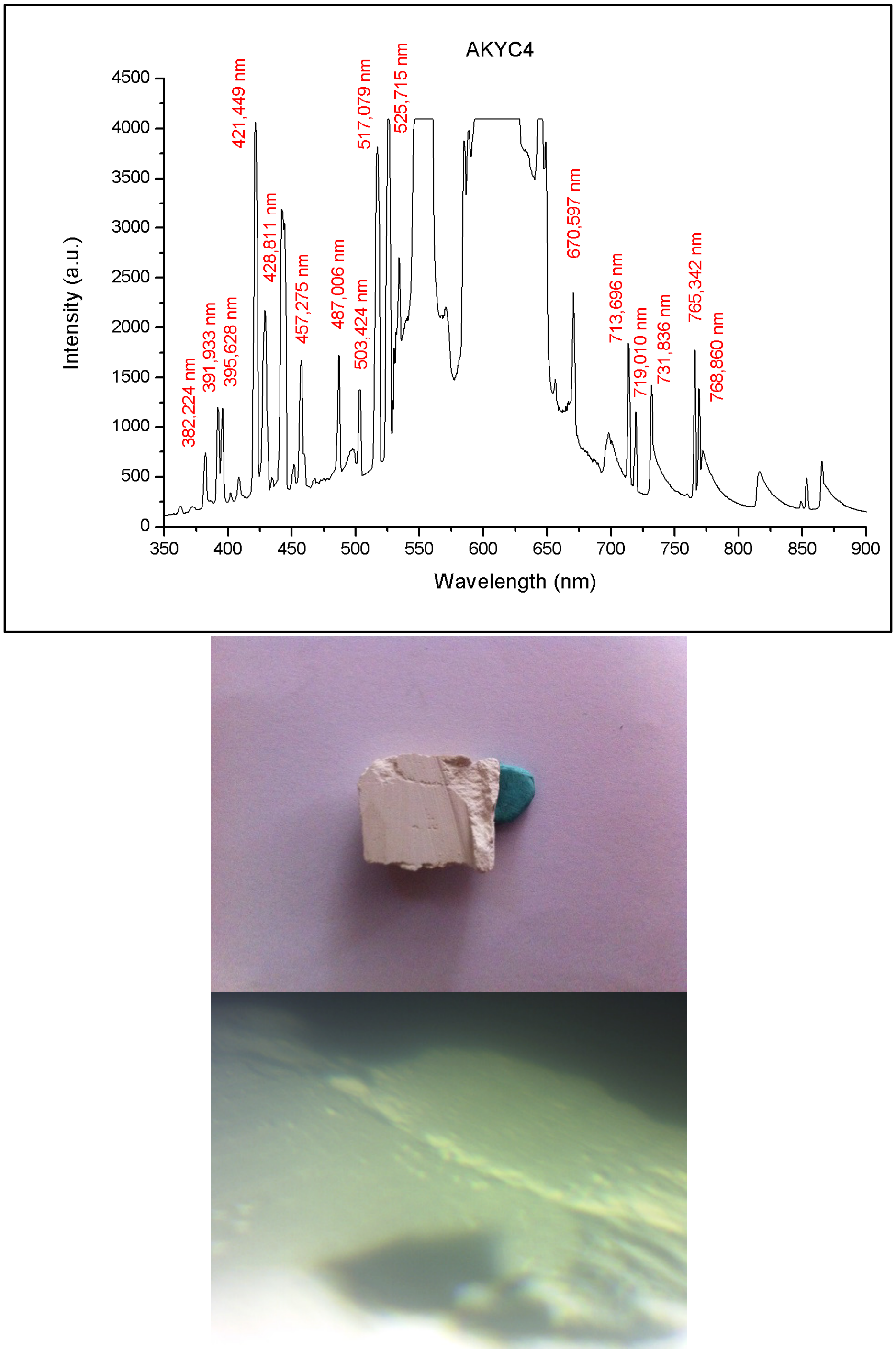

Figure 3.21 LIBS spectrum and photos of AKYC4

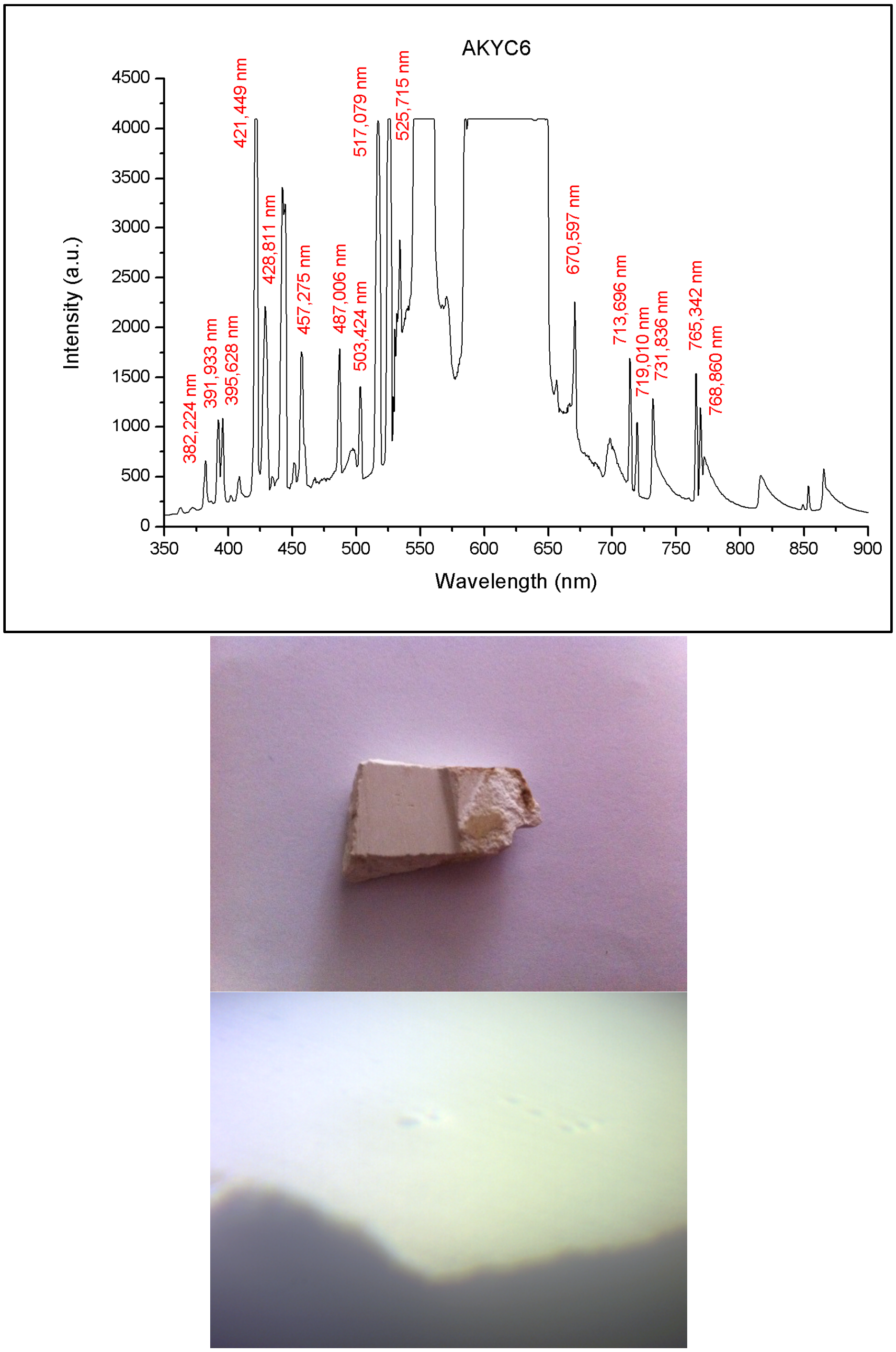

Figure 3.22 LIBS spectrum and photos of AKYC6

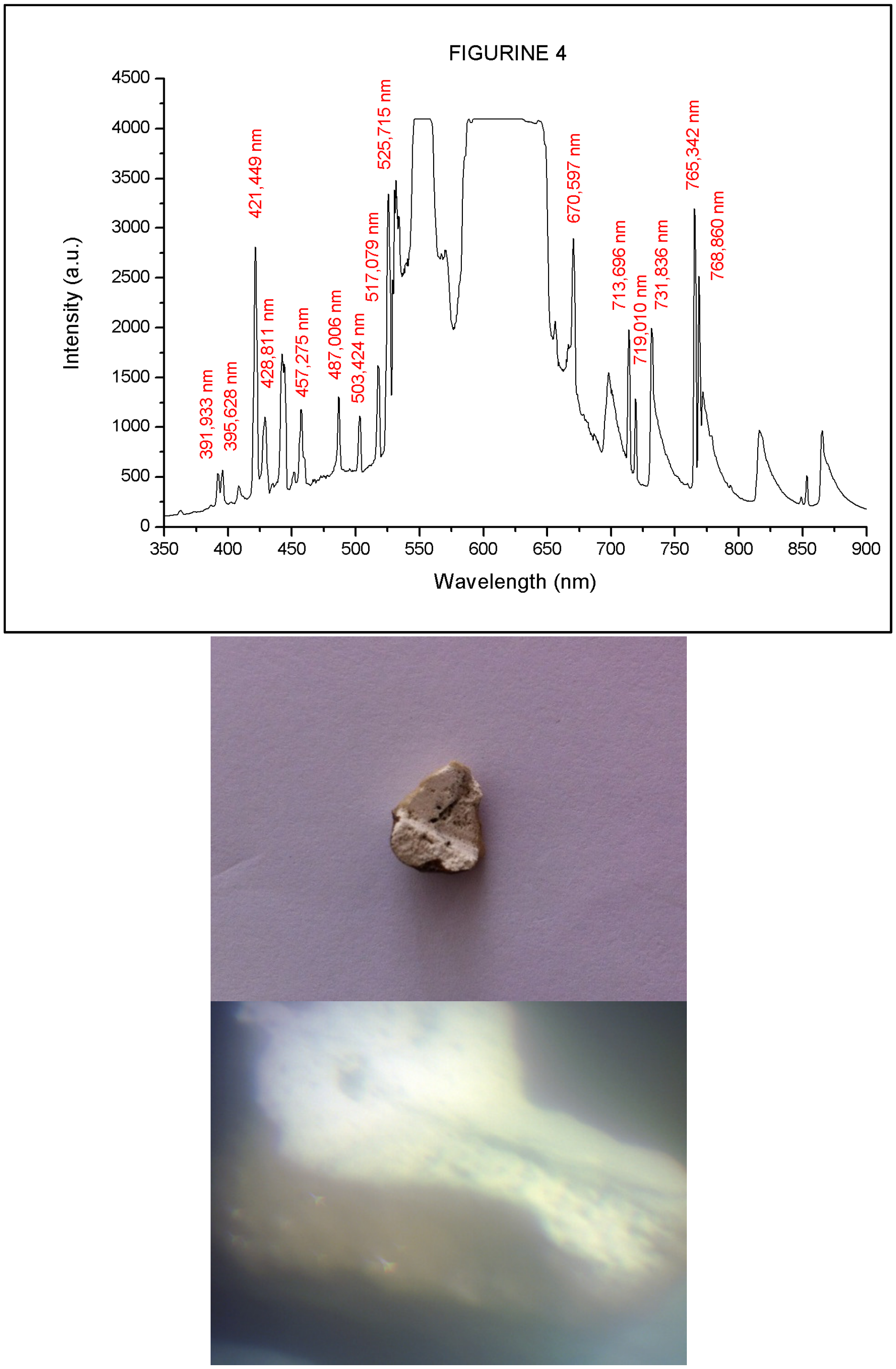

Figure 3.23 LIBS spectrum and photos of FIGURINE4

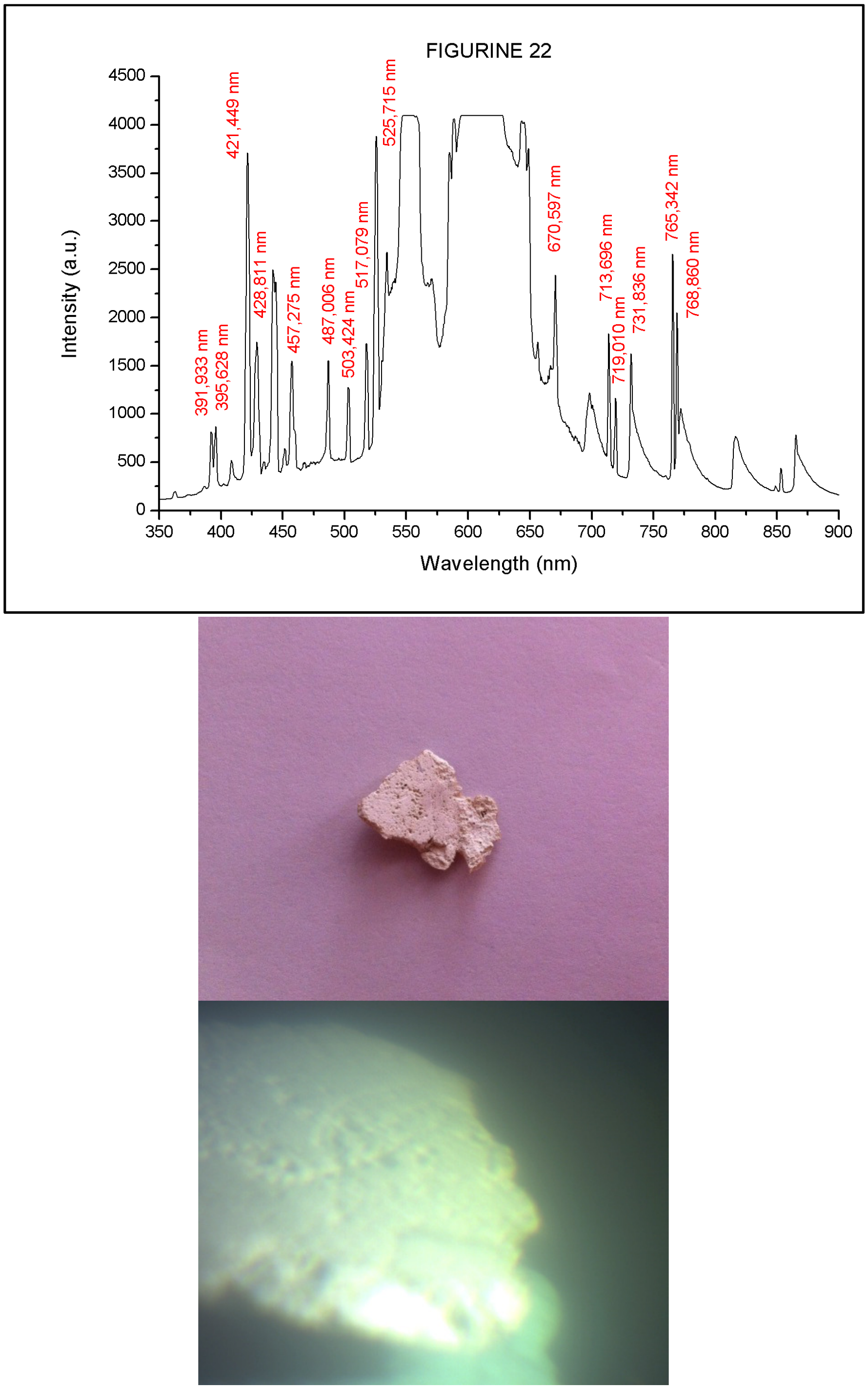

Figure 3.24 LIBS spectrum and photos of FIGURINE22

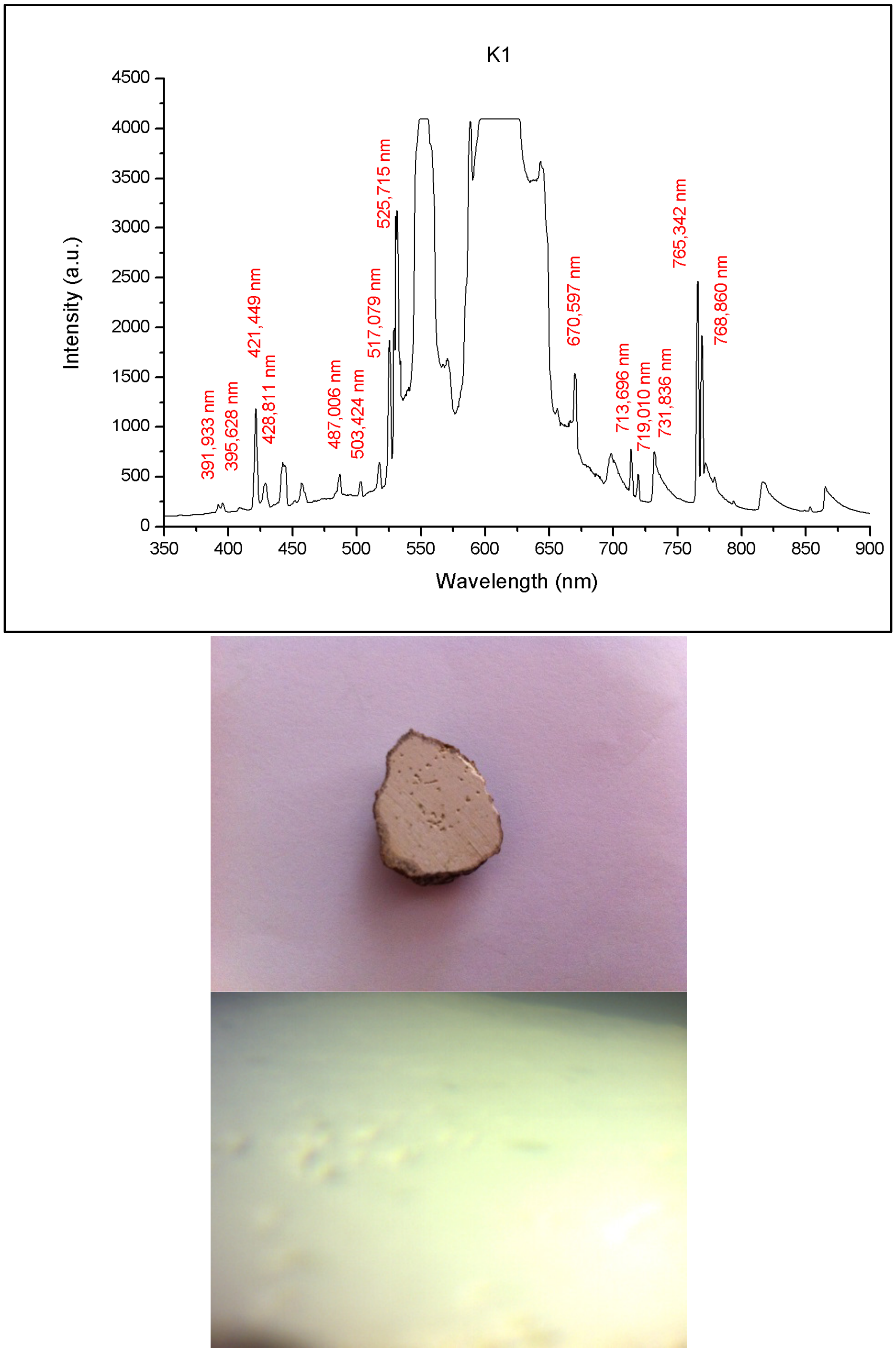

Figure 3.25 LIBS spectrum and photos of K1

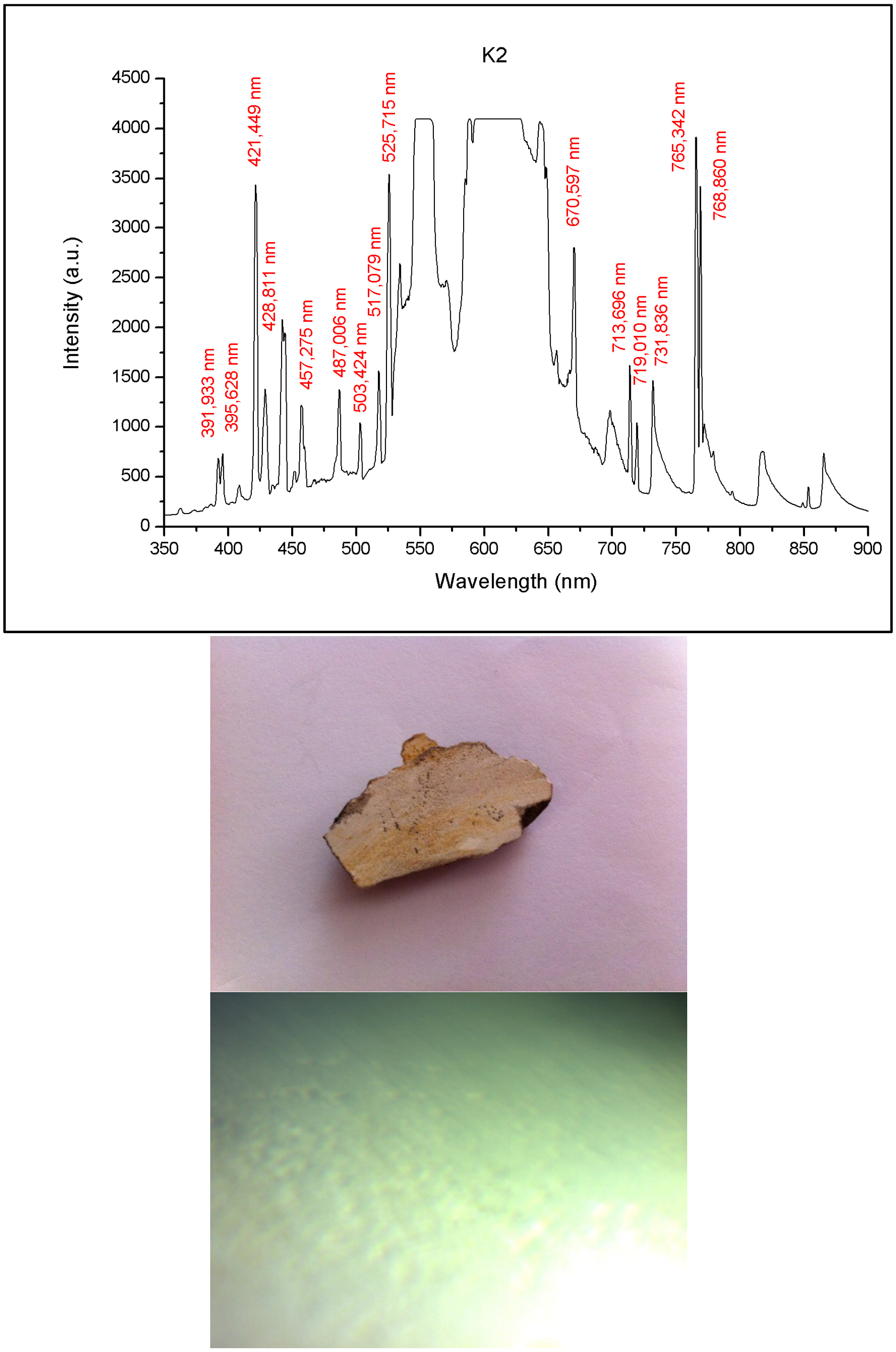

Figure 3.26 LIBS spectrum and photos of K2

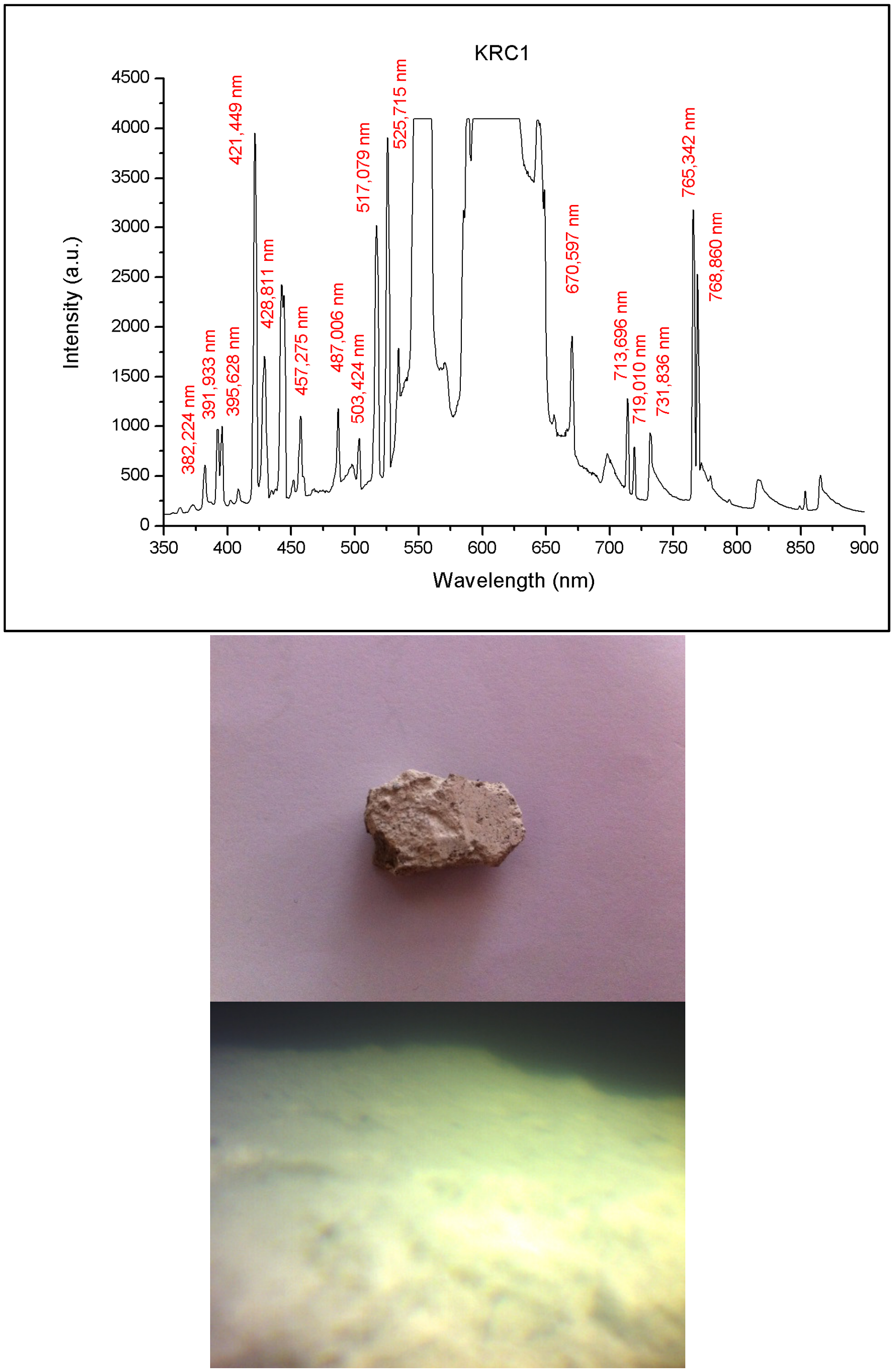

Figure 3.27 LIBS spectrum and photos of KRC1

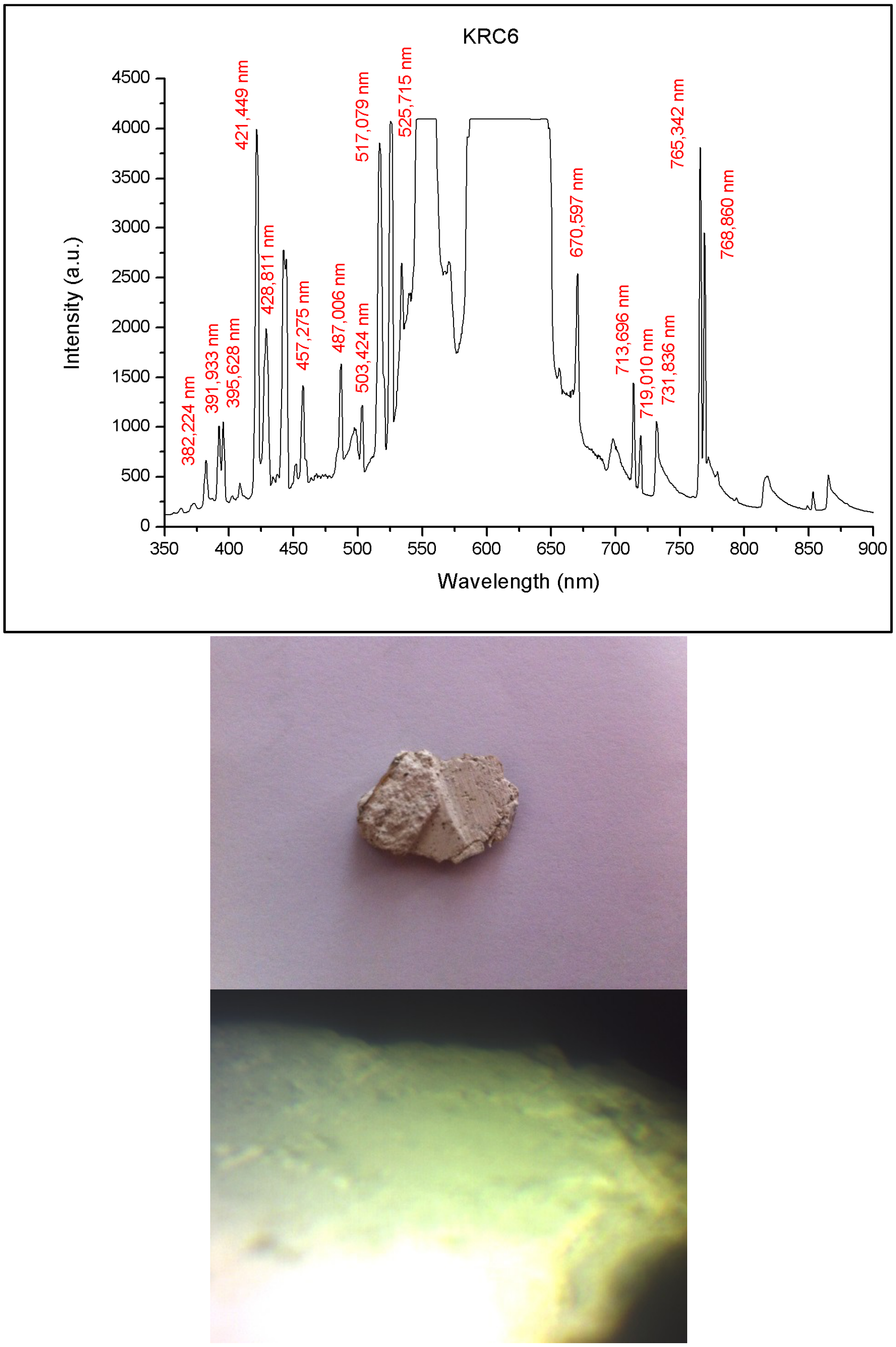

Figure 3.28 LIBS spectrum and photos of KRC6

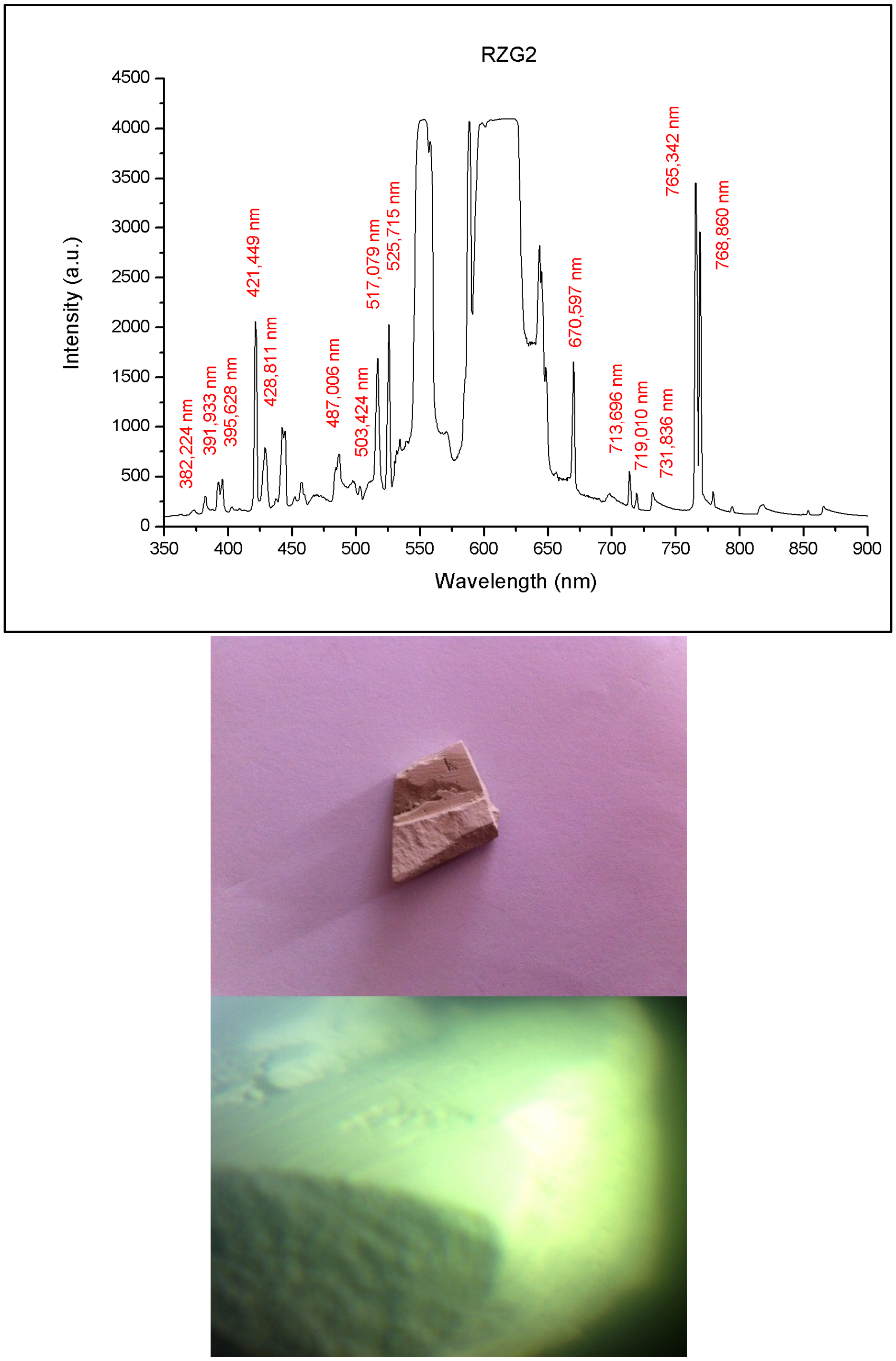

Figure 3.29 LIBS spectrum and photos of RZG2

CHAPTER 4

RESULTS AND DISCUSSIONS

4.1 Signal-to-Noise Ratio (S/N) Calculation

The first work to do with the LIBS data of the archaeological materials is the S/N calculations. With the help of the graphs of intensity vs. wavelength the S/Ns are calculated for every peak having the basic requirements which are having suitable one peak and its two leg. The noise which does not compose of any increase or decrease in intensity near one of the legs and corresponding wavelength range are used in making the graph of the S/N calculation. The procedure of finding S/N is that the tredline of this graph is found as a fourth-degree polynomial function. One should set the corresponding wavelength values as x in this function and obtain y values which should be subtracted from the original y values. Standard deviation (SD) of residual y values or in other name intensity values is calculated. The endpoint intensity values of the legs are added and then divided by two and the result subtracted from the peak intensity value. This final value is divided by SD which gives the S/N value. This process is applied to all the peaks of the LIBS spectra and almost all the S/Ns are found; however, a small number of them did not seen notable due to the problems such as calculating the S/N value less than 1, having very high peak intensity value, being not a real peak or absence of a peak. Figure 4.1 shows the S/N values of the archaeological materials.

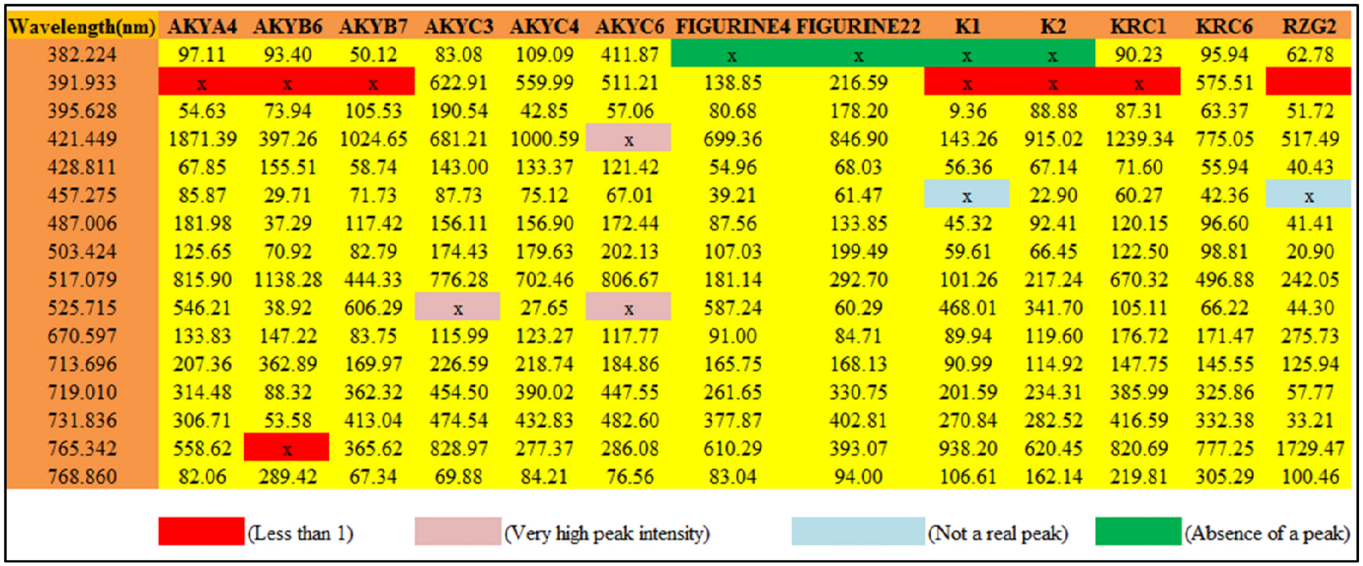

Wavelength(nm)	AKYA4	AKYB6	AKYB7	AKYC3	AKYC4	AKYC6	FIGURINE4	FIGURINE22	K1	K2	KRC1	KRC6	RZG2
382.224	97.11	93.40	50.12	83.08	109.09	411.87	🟩 x	🟩 x	🟩 x	🟩 x	90.23	95.94	62.78
391.933	🟥 x	🟥 x	🟥 x	622.91	559.99	511.21	138.85	216.59	🟥 x	🟥 x	🟥 x	575.51	🟥
395.628	54.63	73.94	105.53	190.54	42.85	57.06	80.68	178.20	9.36	88.88	87.31	63.37	51.72
421.449	1871.39	397.26	1024.65	681.21	1000.59	🟪 x	699.36	846.90	143.26	915.02	1239.34	775.05	517.49
428.811	67.85	155.51	58.74	143.00	133.37	121.42	54.96	68.03	56.36	67.14	71.60	55.94	40.43
457.275	85.87	29.71	71.73	87.73	75.12	67.01	39.21	61.47	🟦 x	22.90	60.27	42.36	🟦 x
487.006	181.98	37.29	117.42	156.11	156.90	172.44	87.56	133.85	45.32	92.41	120.15	96.60	41.41
503.424	125.65	70.92	82.79	174.43	179.63	202.13	107.03	199.49	59.61	66.45	122.50	98.81	20.90
517.079	815.90	1138.28	444.33	776.28	702.46	806.67	181.14	292.70	101.26	217.24	670.32	496.88	242.05
525.715	546.21	38.92	606.29	🟪 x	27.65	🟪 x	587.24	60.29	468.01	341.70	105.11	66.22	44.30
670.597	133.83	147.22	83.75	115.99	123.27	117.77	91.00	84.71	89.94	119.60	176.72	171.47	275.73
713.696	207.36	362.89	169.97	226.59	218.74	184.86	165.75	168.13	90.99	114.92	147.75	145.55	125.94
719.010	314.48	88.32	362.32	454.50	390.02	447.55	261.65	330.75	201.59	234.31	385.99	325.86	57.77
731.836	306.71	53.58	413.04	474.54	432.83	482.60	377.87	402.81	270.84	282.52	416.59	332.38	33.21
765.342	558.62	🟥 x	365.62	828.97	277.37	286.08	610.29	393.07	938.20	620.45	820.69	777.25	1729.47
768.860	82.06	289.42	67.34	69.88	84.21	76.56	83.04	94.00	106.61	162.14	219.81	305.29	100.46

🟥 (Less than 1) 🟪 (Very high peak intensity) 🟦 (Not a real peak) 🟩 (Absence of a peak)

Figure 4.1 S/N values of archaeological materials

4.2 Qualitative LIBS Data Analysis

In the study of Üftade Muşkara [17], many elements were detected by utilizing Inductively Coupled Plasma Optical Emission Spectrometry (ICP-OES) and Inductively Coupled Plasma Mass Spectrometry (ICP-MS) on the archaeological materials. The identified elements contain Rare Earth Elements (REEs) listed in figure 4.2 which cannot be detected via LIBS. Therefore, detecting the elements which are not REEs is the main aim of the LIBS experiments.

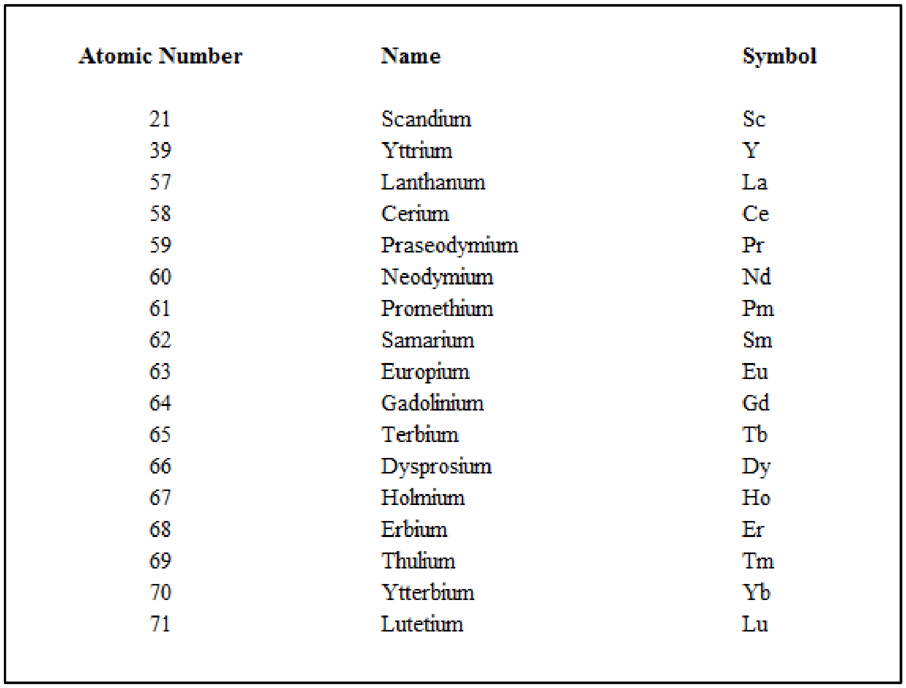

Atomic Number	Name	Symbol
21	Scandium	Sc
39	Yttrium	Y
57	Lanthanum	La
58	Cerium	Ce
59	Praseodymium	Pr
60	Neodymium	Nd
61	Promethium	Pm
62	Samarium	Sm
63	Europium	Eu
64	Gadolinium	Gd
65	Terbium	Tb
66	Dysprosium	Dy
67	Holmium	Ho
68	Erbium	Er
69	Thulium	Tm
70	Ytterbium	Yb
71	Lutetium	Lu

Figure 4.2 Rare Earth Elements (REEs)

Mg, Fe, Mn, Sr, Ba and Cr are the elements which are not REEs detected in the archaeological materials in the study of Üftade Muşkara [17] and thus they are the target elements in the LIBS measurements.

The software program whose task is to store the database about spectral lines of elements and specify the persistent lines of elements helps to decide which line can be able to belong which element. According to the software database, whose one example is shown in figure 4.3, among all the lines found from the archaeological materials, the wavelengths of 382.224 nm, 421.449 nm, 428.811 nm and 517.079 nm represent Mg (I) (first ionization), Sr (II) (second ionization), Cr (I) (first ionization) and Mg (I) (first ionization) respectively. In addition, in order to ensure these results, the National Institute of Standards and Technology (NIST) database was checked [27-29] and it is proved that these lines are the persistent lines of these elements. On the other hand, in the all graphs of the archaeological materials, the most obvious two Potassium (K) lines are seen as the wavelengths of 765.342 nm and 768.860 nm very clearly.

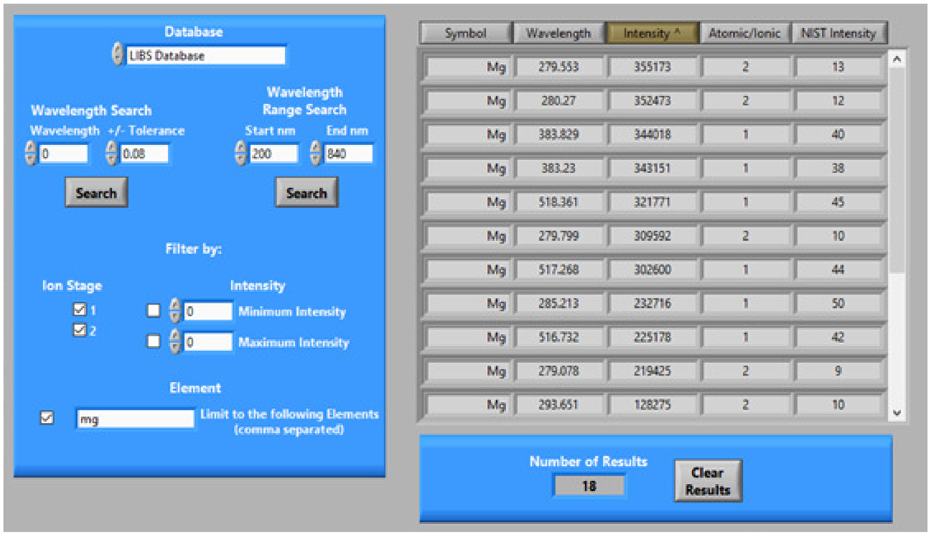

Database: LIBS Database

Wavelength: 0

+/- Tolerance: 0.08

Start nm: 200

End nm: 840

Ion Stage: ☑ 1 ☑ 2

☐ 0 Minimum Intensity

☐ 0 Maximum Intensity

☑ mg Limit to the following Elements (comma separated)

Symbol	Wavelength	Intensity ^	Atomic/Ionic	NIST Intensity
Mg	279.553	355173	2	13
Mg	280.27	352473	2	12
Mg	383.829	344018	1	40
Mg	383.23	343151	1	38
Mg	518.361	321771	1	45
Mg	279.799	309592	2	10
Mg	517.268	302600	1	44
Mg	285.213	232716	1	50
Mg	516.732	225178	1	42
Mg	279.078	219425	2	9
Mg	293.651	128275	2	10

Number of Results: 18

Figure 4.3 Example of database search from software program

4.3 Limit of Detection (LOD) Calculation

The next step is the LOD calculations of the elements Mg (517 nm), Sr (421 nm) and Cr (428 nm) that detected qualitatively. In order to find the LODs, one should know the lowest concentration values of these elements which are obtained from the results of the study by Üftade Muşkara [17] in the unit of mg/kg. This information also tells that in which archaeological materials these concentration values are observed. The other requirement to find the LODs is the corresponding S/Ns given in figure 4.1. The mathematical formula to find LOD is given below:

$$\frac{3\ *\ (the\ lowest\ concentration\ value)}{(the\ corresponding\ \frac{S}{N}\ value)}$$

Figure 4.4 presents the LOD values of the elements Mg, Sr and Cr and other necessary information used in the LOD calculations. It is seen in figure 4.4 that the LOD values are quite low.

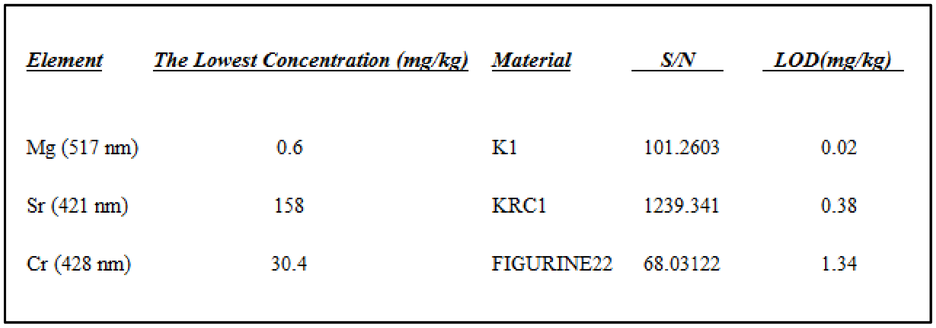

Element	*The Lowest Concentration (mg/kg)*	*Material*	*S/N*	*LOD(mg/kg)*
Mg (517 nm)	0.6	K1	101.2603	0.02
Sr (421 nm)	158	KRC1	1239.341	0.38
Cr (428 nm)	30.4	FIGURINE22	68.03122	1.34

Figure 4.4 LOD values of elements Mg, Sr and Cr

Although it is not too critical, the reason why the S/N value at 517 nm line is used for Mg in its LOD calculation is the absence of a peak at 382 nm for the archaeological material K1 and thus at that point the S/N value cannot be calculated seen in figure 4.1. Many spectral lines of an element can be detected and analyzed; however, there is always only one LOD value for one element.

4.4 Quantitative LIBS Data Analysis

The last part of the LIBS data analyses is the quantitative analysis. In this part, the method of calibration curve is utilized and the aim of this method is to see how the intensity or in a similar meaning area under peak changes depending on the concentration of the constituent in a material. The construction of the calibration curves for the elements Mg, Sr and Cr consists of two steps. First of all, for the each line of 517 nm (Mg (I)), 421 nm (Sr (II)) and 428 nm (Cr (I)), the peak intensity and area under peak values are gathered by using the LIBS spectra data of the archaeological materials that can be seen in figure 4.5. The last step is obtaining the all concentration values for the constituents Mg, Sr and Cr found in the archaeological materials. The concentration values in the unit of mg/kg are taken from the study of Üftade Muşkara [17] as well and can be seen in figure 4.6.

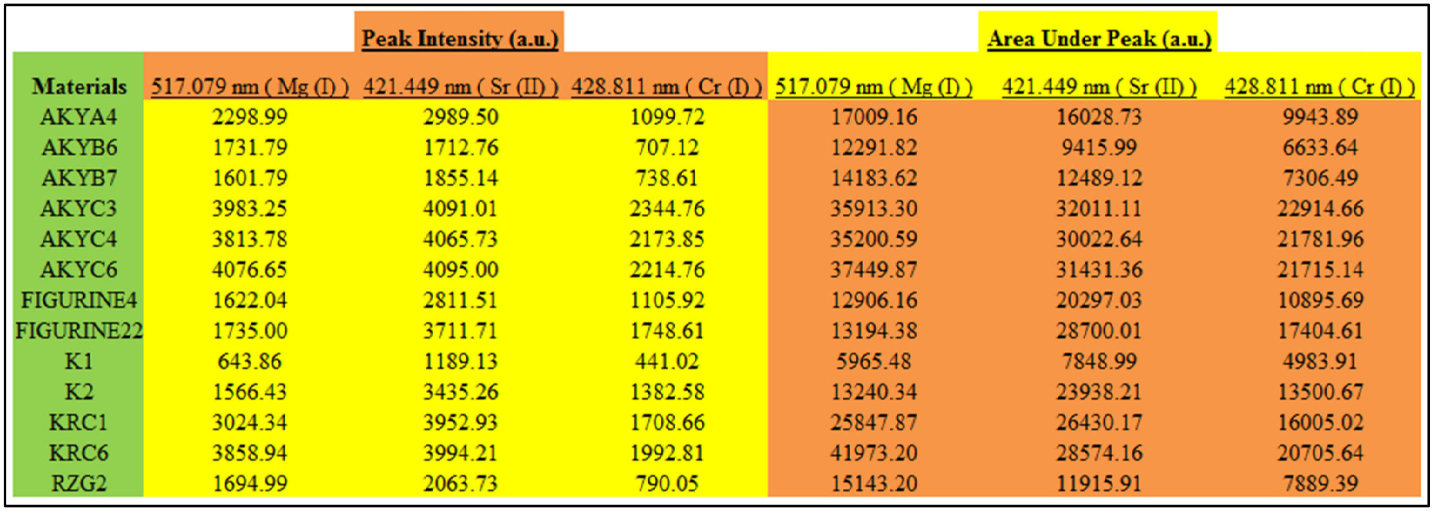

Materials	Peak Intensity (a.u.)			Area Under Peak (a.u.)		
	517.079 nm (Mg (I))	421.449 nm (Sr (II))	428.811 nm (Cr (I))	517.079 nm (Mg (I))	421.449 nm (Sr (II))	428.811 nm (Cr (I))
AKYA4	2298.99	2989.50	1099.72	17009.16	16028.73	9943.89
AKYB6	1731.79	1712.76	707.12	12291.82	9415.99	6633.64
AKYB7	1601.79	1855.14	738.61	14183.62	12489.12	7306.49
AKYC3	3983.25	4091.01	2344.76	35913.30	32011.11	22914.66
AKYC4	3813.78	4065.73	2173.85	35200.59	30022.64	21781.96
AKYC6	4076.65	4095.00	2214.76	37449.87	31431.36	21715.14
FIGURINE4	1622.04	2811.51	1105.92	12906.16	20297.03	10895.69
FIGURINE22	1735.00	3711.71	1748.61	13194.38	28700.01	17404.61
K1	643.86	1189.13	441.02	5965.48	7848.99	4983.91
K2	1566.43	3435.26	1382.58	13240.34	23938.21	13500.67
KRC1	3024.34	3952.93	1708.66	25847.87	26430.17	16005.02
KRC6	3858.94	3994.21	1992.81	41973.20	28574.16	20705.64
RZG2	1694.99	2063.73	790.05	15143.20	11915.91	7889.39

Figure 4.5 Peak intensity and area under peak values of archaeological materials

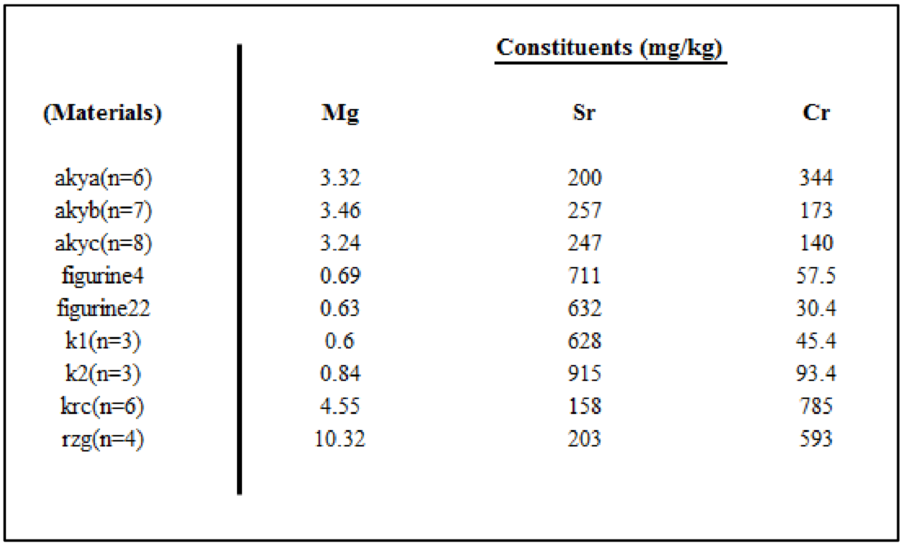

		Constituents (mg/kg)	
(Materials)	Mg	Sr	Cr
akya(n=6)	3.32	200	344
akyb(n=7)	3.46	257	173
akyc(n=8)	3.24	247	140
figurine4	0.69	711	57.5
figurine22	0.63	632	30.4
k1(n=3)	0.6	628	45.4
k2(n=3)	0.84	915	93.4
krc(n=6)	4.55	158	785
rzg(n=4)	10.32	203	593

Figure 4.6 Concentration values of constituents Mg, Sr and Cr

In figure 4.6, it is seen that there are n values in parentheses and Üftade Muşkara uses this to inform the readers about the number of related archaeological material in her study [17]. For illustration, if there are eight pieces of AKYC that can be seen in figure 4.6 as (n = 8), the two of them AKYC3 and AKYC4 are picked up to be measured and analyzed in the LIBS set-up.

From now on, the calibration curves are ready to be constructed. The most appropriate three or four data points both for the peak intensity and area under peak are selected from the LIBS spectra data and concentration values of the constituents Mg, Sr and Cr to fit their calibration graphs linearly. In addition, these data points are named as the primary data. The calibration process is divided into four parts and the aim is achieving the best calibration curves for the constituents Mg, Sr and Cr because there are matrix effects which decrease the quality of the calibration curves and make them nonlinear. Therefore, these matrix effects should be eliminated by some normalization techniques. In the calibration graphs of the every part, the same x values that are the concentration values of the constituents are used, whereas the y values that are processed to eliminate the matrix effects differ and these y values are named as the predicted concentrations. In the first part, the first calibration curve is constructed with the primary data that is not subjected to any manipulation. In the second part, the y values coming from the primary data are divided by the slope of their first calibration curve. In the third part, the y values again coming from the primary data are divided by their background intensity. Lastly, in the fourth part, the same y values are divided by their OH emission band area. The example of OH emission band area from Figurine4 is seen in figure 4.7.

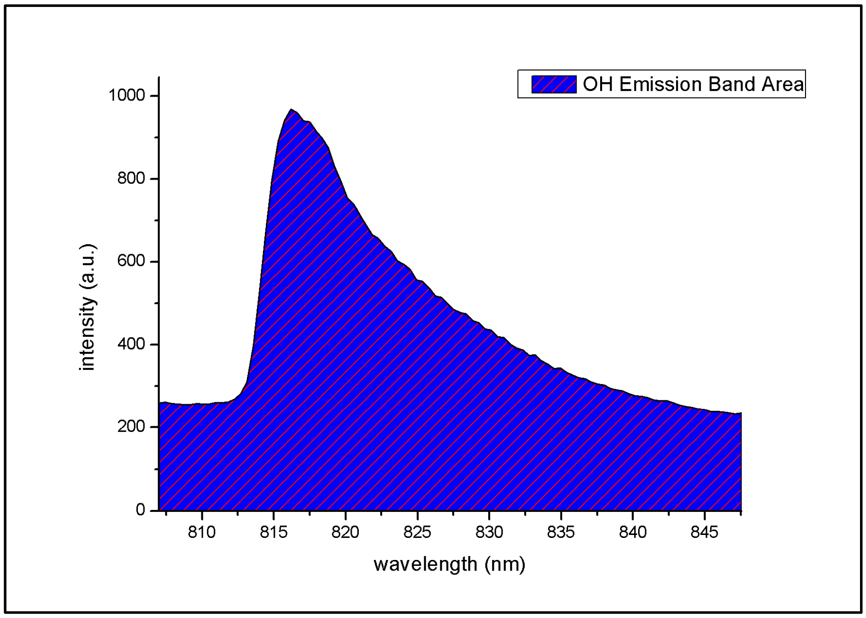

Figure 4.7 Example of OH emission band area

The first part and other three calibration techniques are applied to the data points of the constituents Mg, Sr and Cr in order to see how their calibration curves are affected and whether the matrix effects are resolved or not. Their calibration curves both for the peak intensity and area under peak are represented in figures 4.8-13. The numerical values of these calibration curves and their normalization techniques are presented in the appendix part.

The calibration curves for the constituents Mg, Sr and Cr show quantitatively that the most effective calibration technique that provides a good linear fit is dividing the y values by their OH emission band area and after that using their background intensity as a denominator is coming, whereas dividing the y values with the slope of their first calibration curve cannot have noticeable effects on the calibration curves.

In the normalization techniques, for the each constituent, the background intensities and OH emission band areas are obtained from the LIBS spectra data of the constituents.

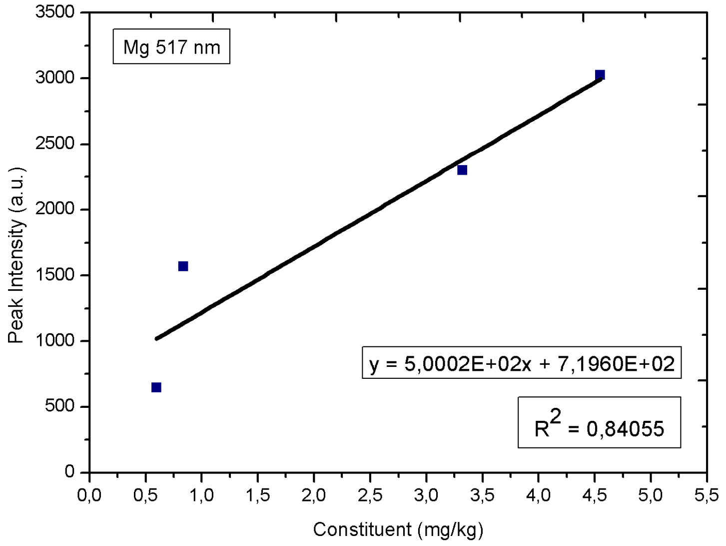
Mg 517 nm
Peak Intensity (a.u.)
Constituent (mg/kg)
y = 5,0002E+02x + 7,1960E+02
R^2 = 0,84055
0
500
1000
1500
2000
2500
3000
3500
0,0
0,5
1,0
1,5
2,0
2,5
3,0
3,5
4,0
4,5
5,0
5,5

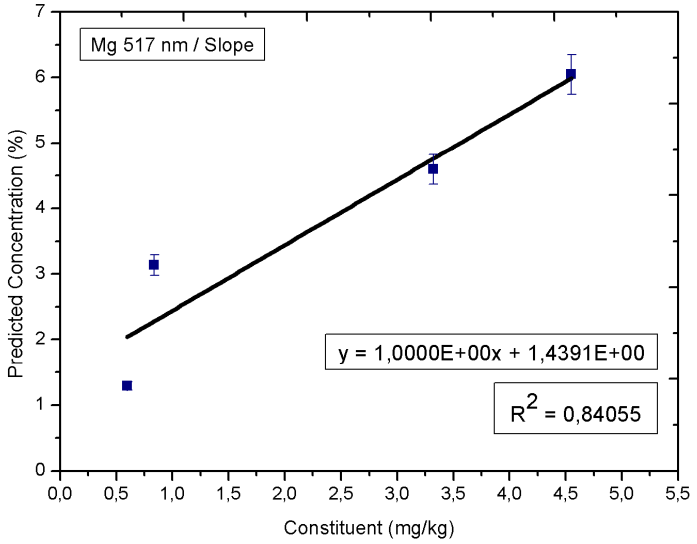
Mg 517 nm / Slope
Predicted Concentration (%)
Constituent (mg/kg)
y = 1,0000E+00x + 1,4391E+00
R^2 = 0,84055
0
1
2
3
4
5
6
7
0,0
0,5
1,0
1,5
2,0
2,5
3,0
3,5
4,0
4,5
5,0
5,5

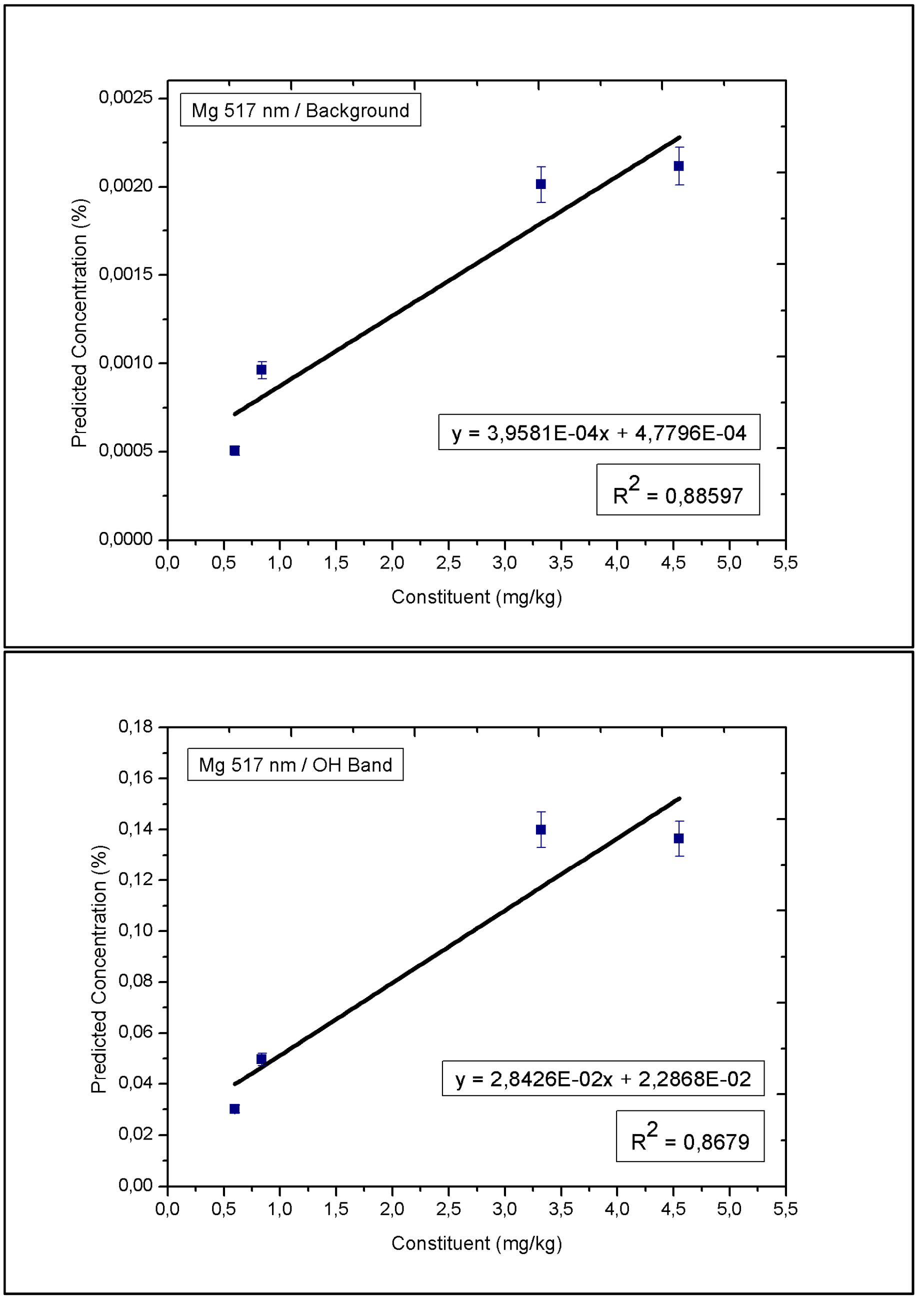

Figure 4.8 Calibration curves of Mg (517 nm) for peak intensity

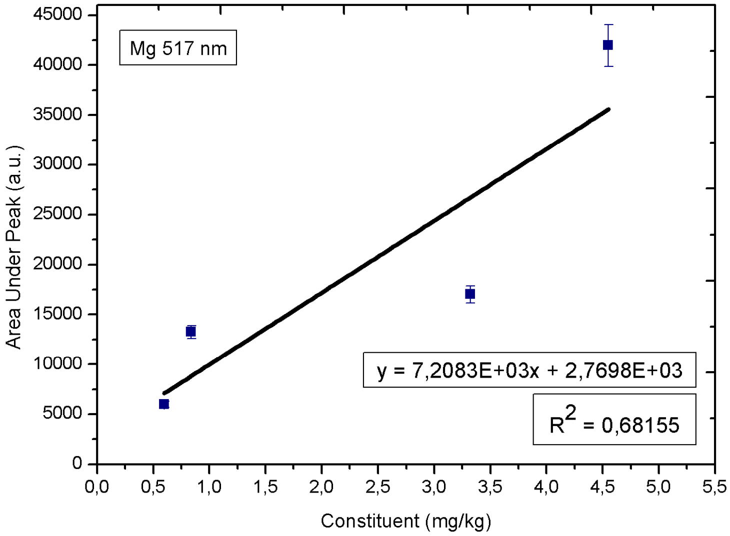
Mg 517 nm
Area Under Peak (a.u.)
45000
40000
35000
30000
25000
20000
15000
10000
5000
0
0,0
0,5
1,0
1,5
2,0
2,5
3,0
3,5
4,0
4,5
5,0
5,5
Constituent (mg/kg)
y = 7,2083E+03x + 2,7698E+03
R^2 = 0,68155

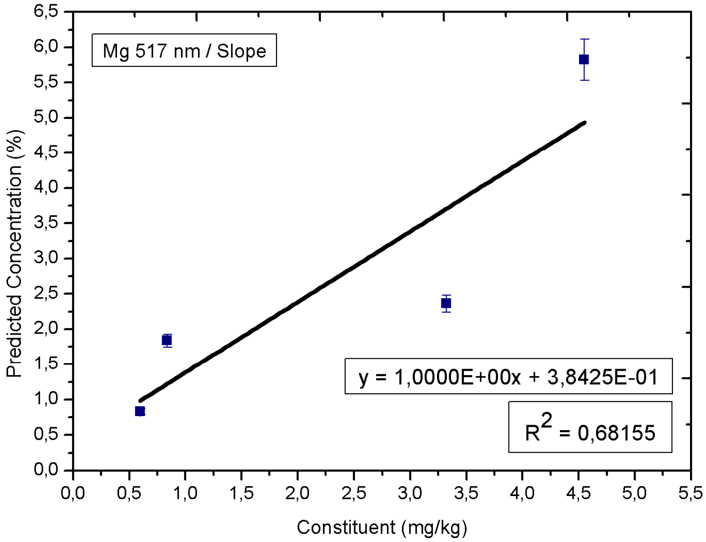
Mg 517 nm / Slope
Predicted Concentration (%)
6,5
6,0
5,5
5,0
4,5
4,0
3,5
3,0
2,5
2,0
1,5
1,0
0,5
0,0
0,0
0,5
1,0
1,5
2,0
2,5
3,0
3,5
4,0
4,5
5,0
5,5
Constituent (mg/kg)
y = 1,0000E+00x + 3,8425E-01
R^2 = 0,68155

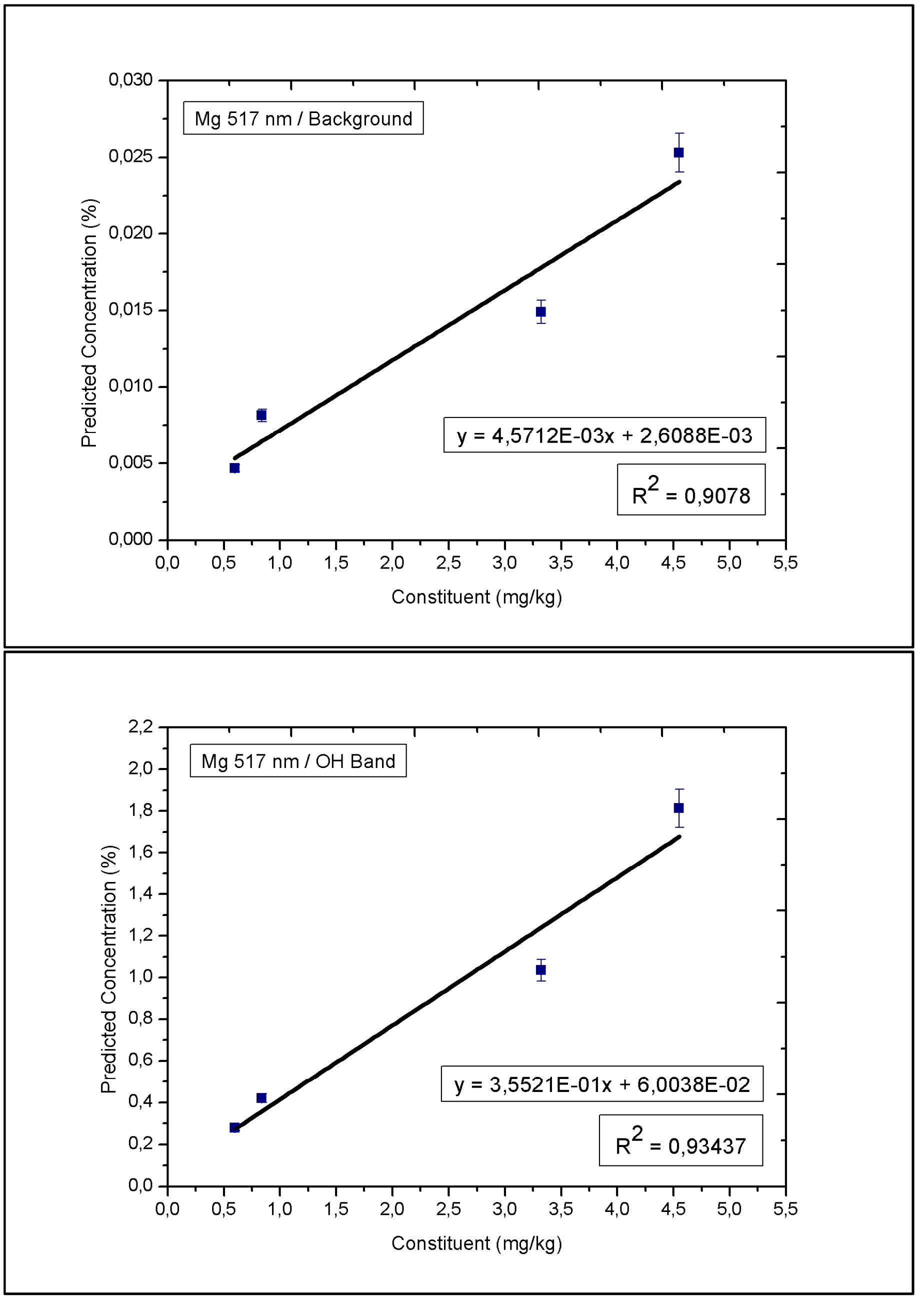

Figure 4.9 Calibration curves of Mg (517 nm) for area under peak

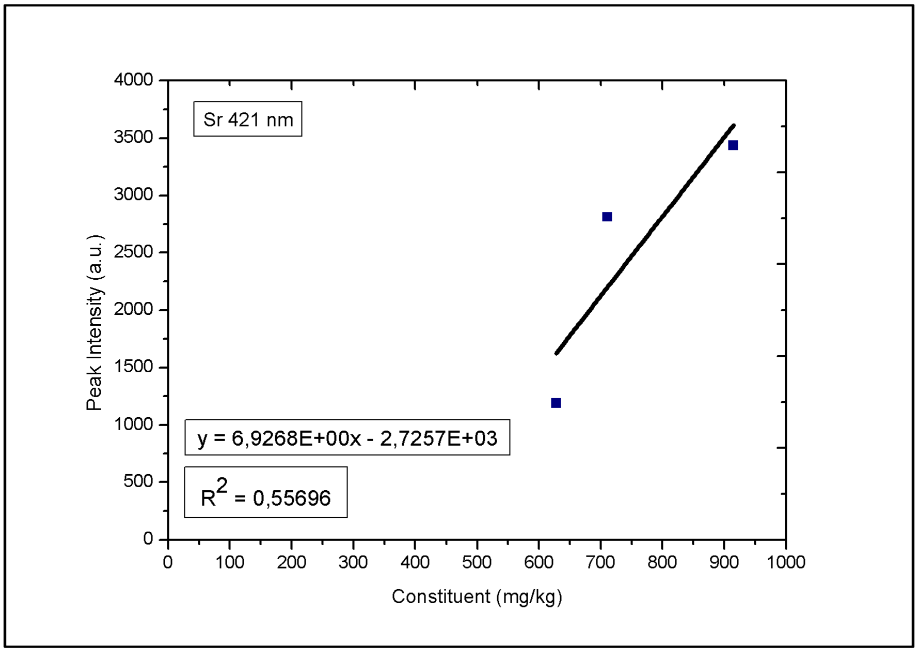
Sr 421 nm
y = 6,9268E+00x - 2,7257E+03
R^2 = 0,55696
Peak Intensity (a.u.)
Constituent (mg/kg)
0
500
1000
1500
2000
2500
3000
3500
4000
0
100
200
300
400
500
600
700
800
900
1000

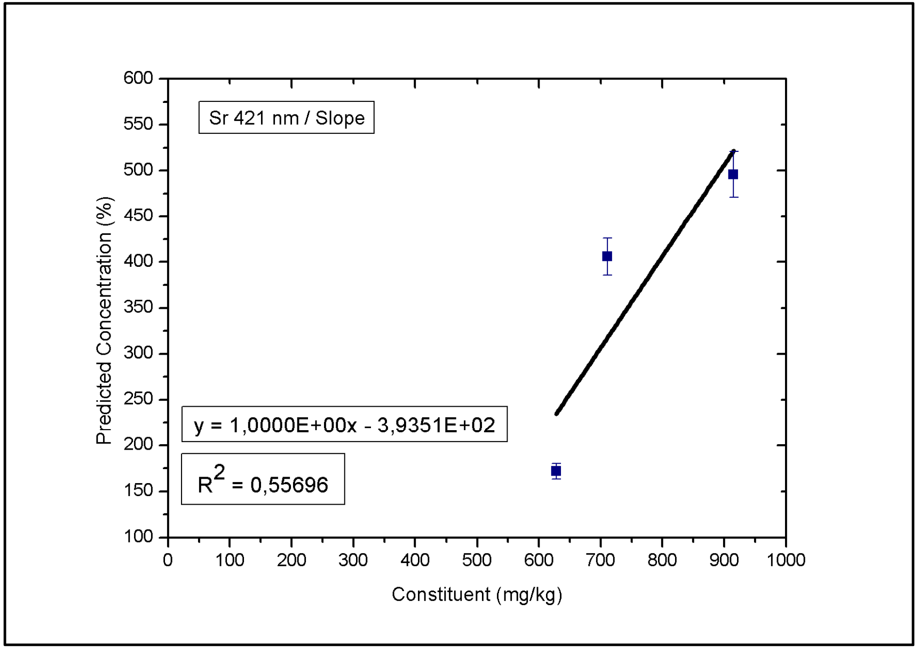
Sr 421 nm / Slope
y = 1,0000E+00x - 3,9351E+02
R^2 = 0,55696
Predicted Concentration (%)
Constituent (mg/kg)
100
150
200
250
300
350
400
450
500
550
600
0
100
200
300
400
500
600
700
800
900
1000

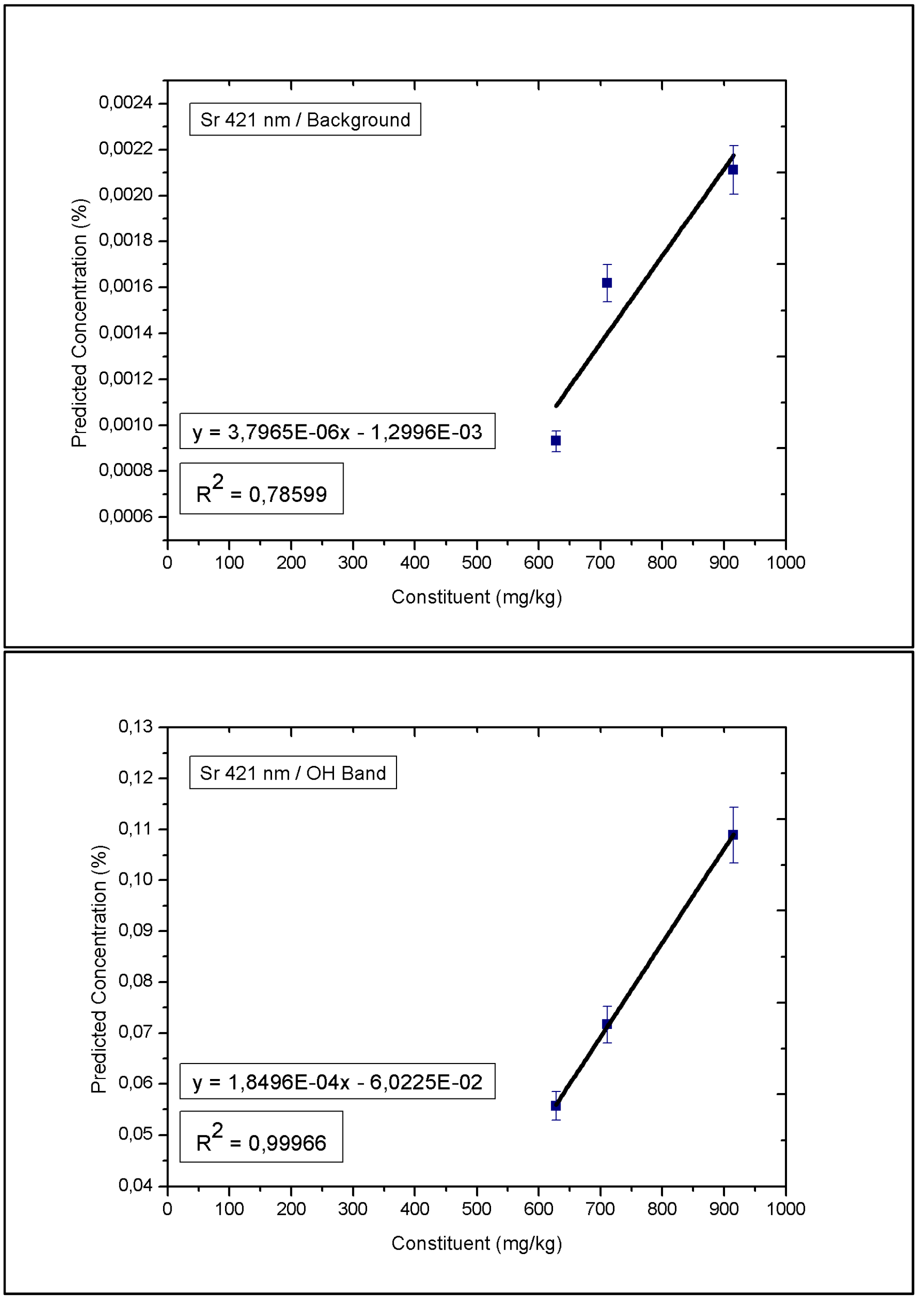

Figure 4.10 Calibration curves of Sr (421 nm) for peak intensity

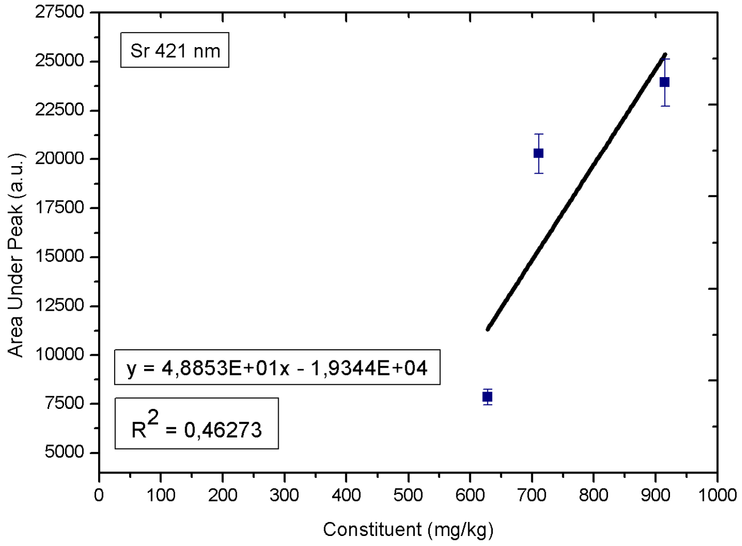
Sr 421 nm
y = 4,8853E+01x - 1,9344E+04
R^2 = 0,46273
Area Under Peak (a.u.)
27500
25000
22500
20000
17500
15000
12500
10000
7500
5000
0
100
200
300
400
500
600
700
800
900
1000
Constituent (mg/kg)

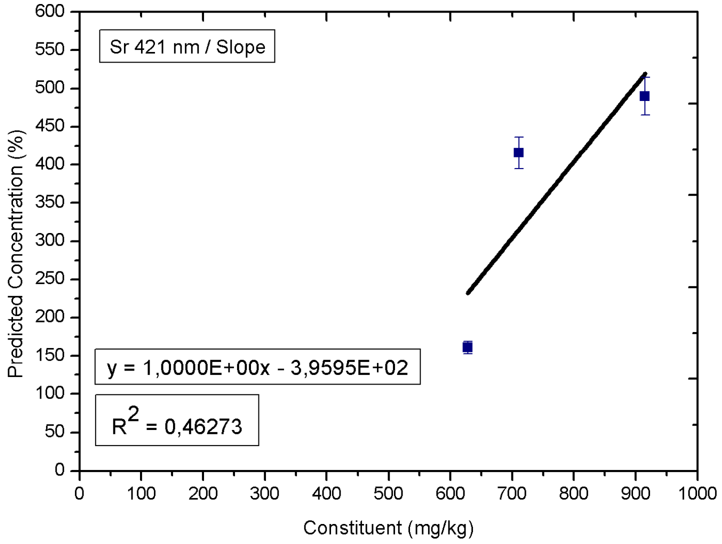
Sr 421 nm / Slope
y = 1,0000E+00x - 3,9595E+02
R^2 = 0,46273
Predicted Concentration (%)
600
550
500
450
400
350
300
250
200
150
100
50
0
100
200
300
400
500
600
700
800
900
1000
Constituent (mg/kg)

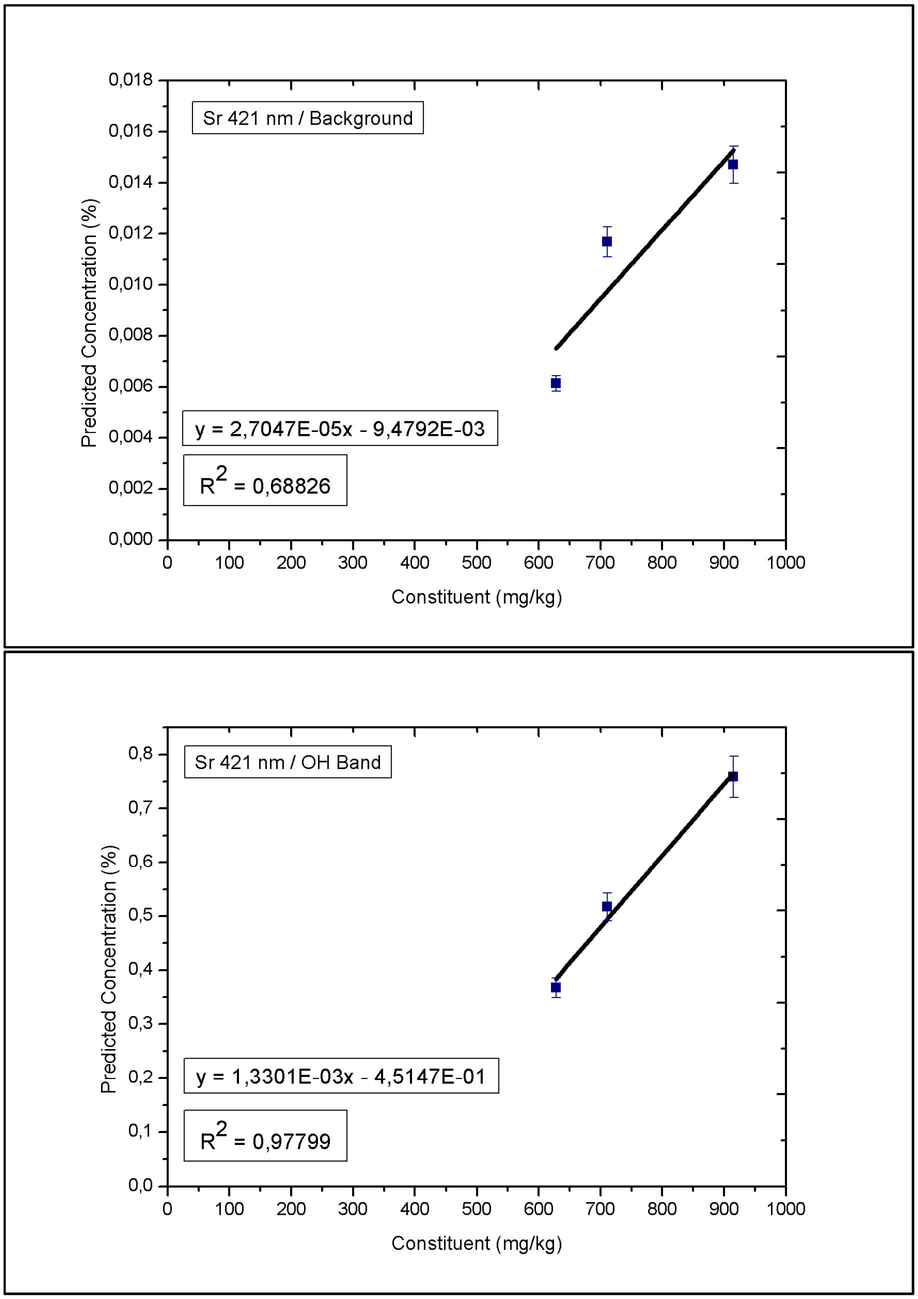

Figure 4.11 Calibration curves of Sr (421 nm) for area under peak

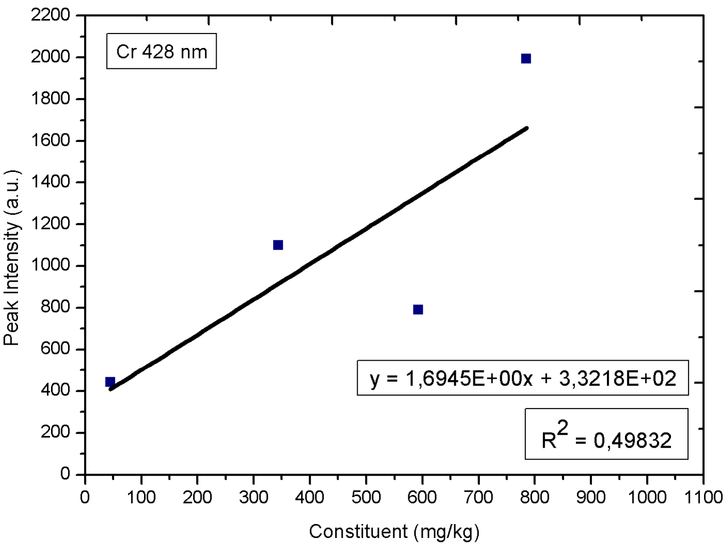
Cr 428 nm
Peak Intensity (a.u.)
0
200
400
600
800
1000
1200
1400
1600
1800
2000
2200
y = 1,6945E+00x + 3,3218E+02
R^2 = 0,49832
0
100
200
300
400
500
600
700
800
900
1000
1100
Constituent (mg/kg)

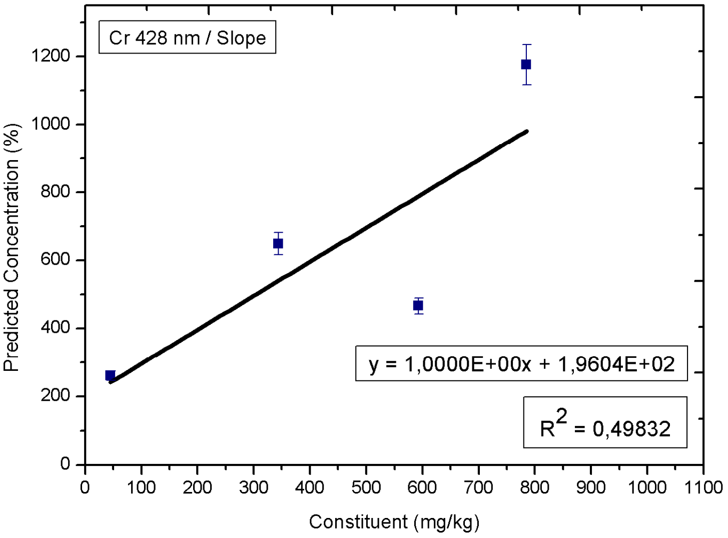
Cr 428 nm / Slope
Predicted Concentration (%)
0
200
400
600
800
1000
1200
y = 1,0000E+00x + 1,9604E+02
R^2 = 0,49832
0
100
200
300
400
500
600
700
800
900
1000
1100
Constituent (mg/kg)

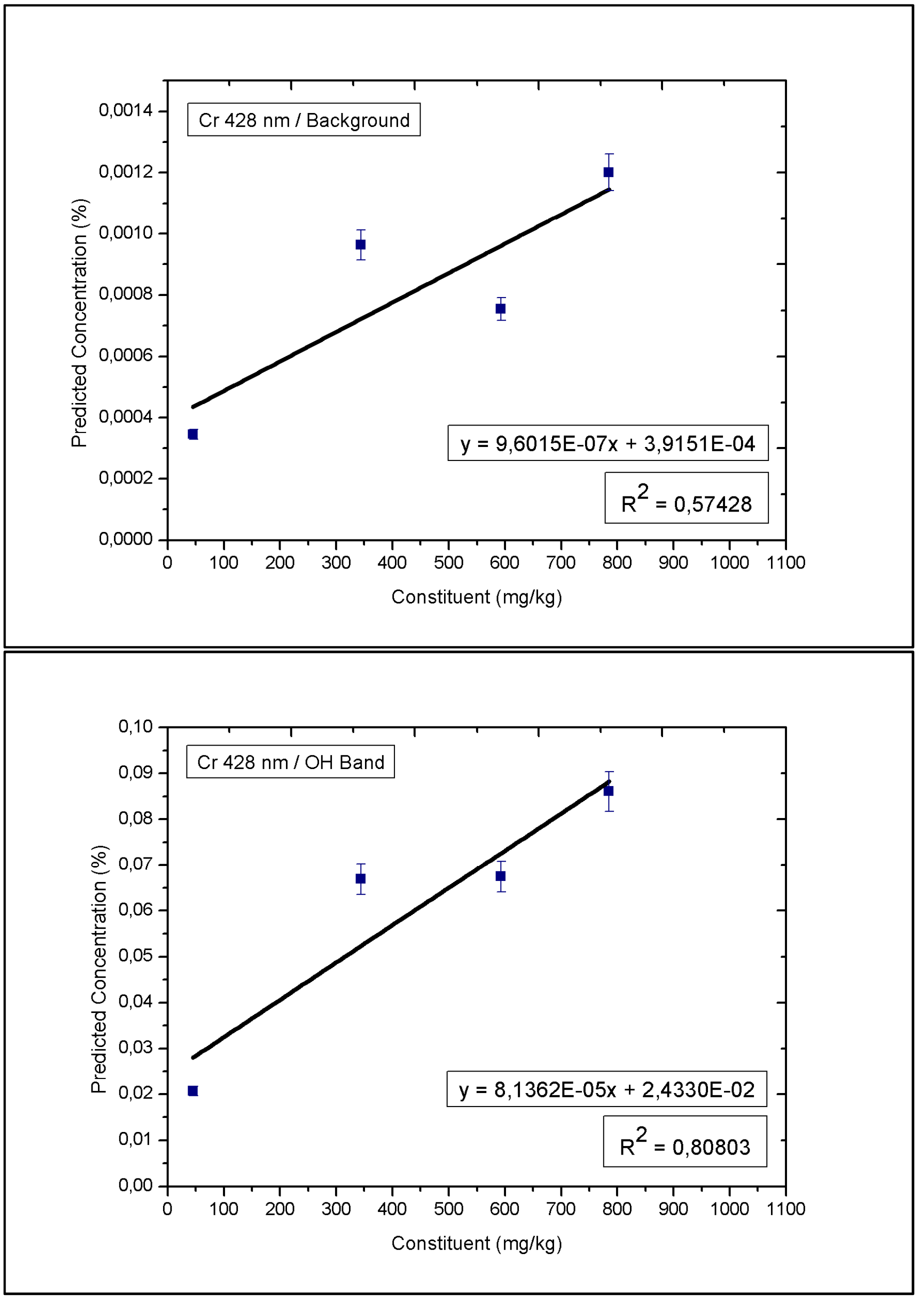

Figure 4.12 Calibration curves of Cr (428 nm) for peak intensity

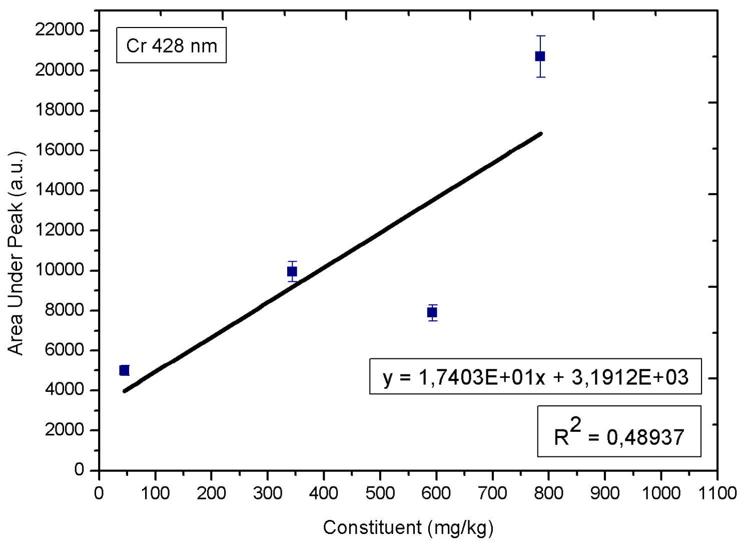
Cr 428 nm
Area Under Peak (a.u.)
0
2000
4000
6000
8000
10000
12000
14000
16000
18000
20000
22000
0
100
200
300
400
500
600
700
800
900
1000
1100
Constituent (mg/kg)
y = 1,7403E+01x + 3,1912E+03
R2 = 0,48937

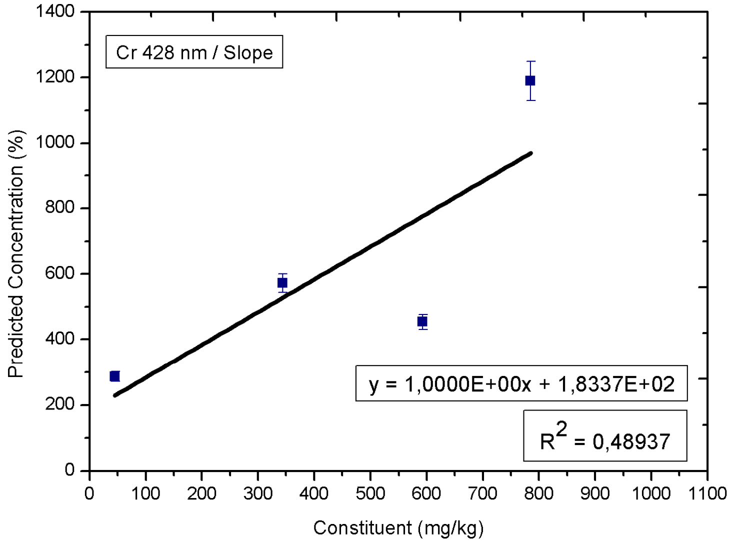
Cr 428 nm / Slope
Predicted Concentration (%)
0
200
400
600
800
1000
1200
1400
0
100
200
300
400
500
600
700
800
900
1000
1100
Constituent (mg/kg)
y = 1,0000E+00x + 1,8337E+02
R2 = 0,48937

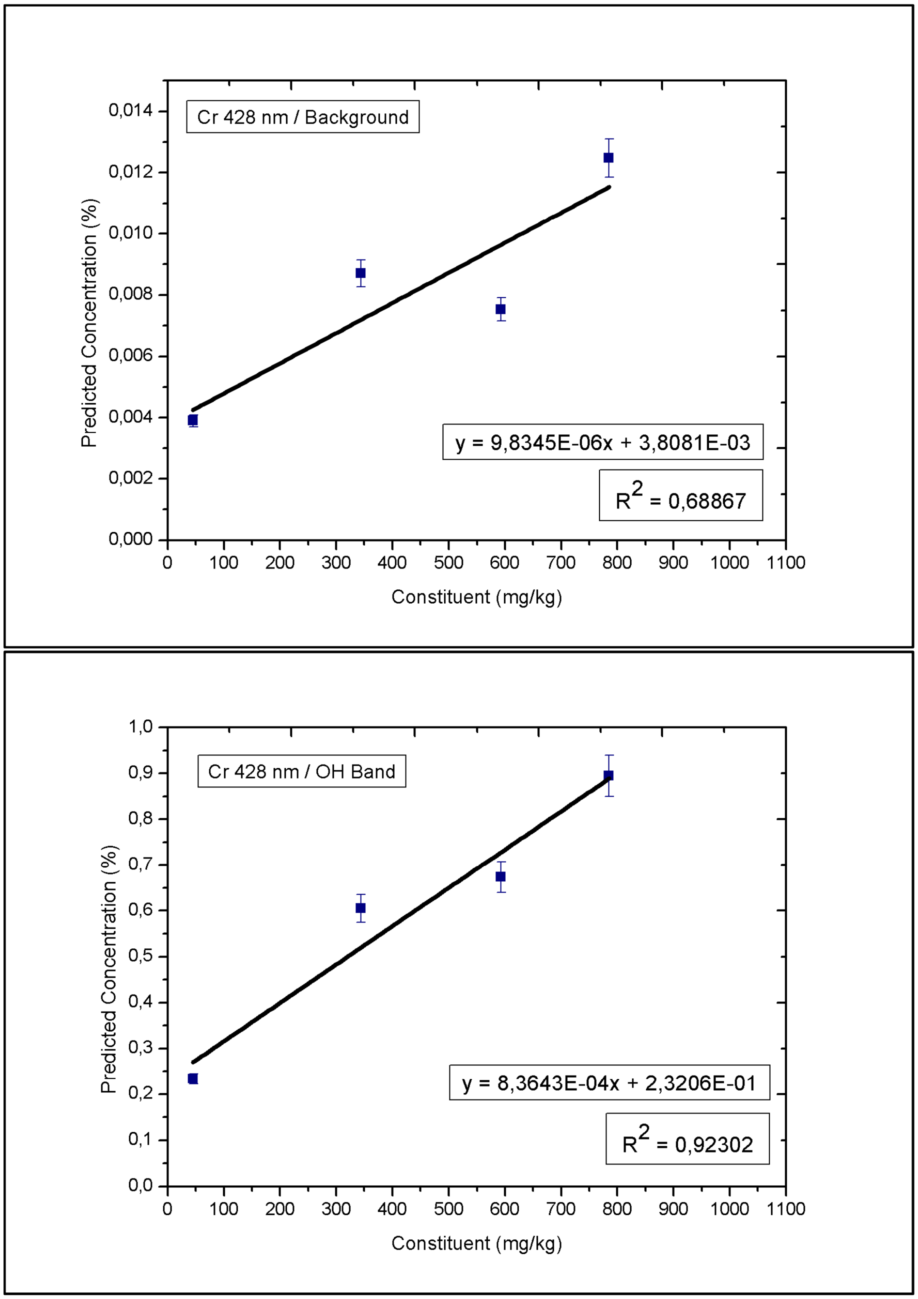

Figure 4.13 Calibration curves of Cr (428 nm) for area under peak

CHAPTER 5

CONCLUSIONS

Laser-Induced Breakdown Spectroscopy (LIBS) showed all its properties in this study. The archaeological materials were not prepared specially. The only thing for the preparation was placing the material surfaces parallel to the optical table and perpendicular to the focused laser pulses. In addition, the LIBS measurement of any archaeological sample was carried out in a very short time that is one second due to the 1 Hz frequency for this study. The camera of the LIBS set-up demonstrated that there were micrometric or milimetric craters formed on the material surfaces due to the plasma creations on them that was the confirmation of the minimal destructiveness of LIBS. As a result of these LIBS properties, the LIBS measurements of the archaeological samples were performed rapidly.

The long section of the LIBS experiments was the analyses of the LIBS data both in qualitative and quantitative ways for the archaeological materials whose names were AKYA4, AKYB(6,7), AKYC(3,4,6), Figuine4, Figurine22, K1, K2, KRC(1,6) and RZG2. The signal-to-noise ratios (S/Ns) were found for every appropriate peak in the graphs of intensity (a.u.) vs. wavelength (nm). Among these peaks, 382.224 nm, 421.449 nm, 428.811 nm and 517.079 nm were labeled qualitatively as Mg (I) (first ionization), Sr (II) (second ionization), Cr (I) (first ionization) and Mg (I) (first ionization) respectively by the help of the related software program database and the National Institute of Standards and Technology (NIST) database. In addition, the most persistent two lines of Potassium (K) 765.342 nm and 768.860 nm were observed distinctly. After representing the existence of the elements Mg, Sr and Cr with their persistent lines found in the LIBS spectra of the archaeological materials, their limit of detection values (LODs) were calculated by using their S/Ns and lowest concentration values. The LODs of the elements Mg, Sr and Cr were found as 0.02, 0.38 and 1.34 in the unit of mg/kg respectively. The LODs were calculated very low which means that the results produced by LIBS could be regarded as successful.

For the information of readers, the archaelogical rock samples and the concentration values of the elements were obtained from the study of the PhD thesis [17] "Characterization Of Emecik Limestone Figurines For Provenance" by Üftade Muşkara.

For the final part of the LIBS analyses, the calibration curve method was utilized in the quantitative analysis section. The peak intensity and area under peak values for the detected elements Mg, Sr and Cr were gathered by using their LIBS spectra and also the other necessary information the concentration values of the elements were collected. This section were divided into four parts to get the best linear fitting in order to eliminate the matrix effects decreasing the quality of the calibration curves and thus making them nonlinear. The first calibration curve graph was constructed with the original y values and x values known as the peak intensity or area under peak values and the concentration values respectively. After this, for the rest of the other parts, the x values remained same and the y values were normalized in several ways. The second graph was made with the original y values divided by the slope of the first graph, the third graph was made with the original y values divided by the related background intensity and the fourth graph was made with the original y values divided by the related OH emission band area. These four calibration techniques were applied to the all determined elements Mg, Sr and Cr in order to make their calibration curves more linear. At the end, it was understood that the most effective calibration technique was dividing the original y values with the related OH emission band area and another good way was using the related background intensity as the denominator for the original y values.

The results have shown that the elemental characterization of the archaeological materials was performed successfully with the LIBS technique. The qualitative and quantitative analyses produced reasonable and effective results. The elements Mg, Sr and Cr were also found to be existed in the archaeological rock samples in the study by Üftade Muşkara [17]. If the experimental LIBS set-up is built up with the high quality equipments, the future works will achieve better results.

For the future works, for illustration, LIBS experiments can be performed in the vacuum that provides to see the spectral lines more distinctly in LIBS spectra. Furthermore, because of the on-time analysis property of LIBS which means that, for example, the measurement obtained in one second due to the laser operating at 1 Hz frequency, LIBS can be applied to the medical operations. Moreover, in the defense industry LIBS can be utilized to detect the hazardous and noxious substances owing to the chance of using LIBS both for laboratory and field experiments.

REFERENCES

[1] Cremers, D. A., & Radziemski, L. J. (2006). *Handbook of Laser-Induced Breakdown Spectroscopy*. Chichester: John Wiley & Sons, Ltd.

[2] Thakur, S. N., & Singh, J. P. (2007). *Laser Induced Breakdown Spectroscopy*. Amsterdam: Elsevier.

[3] Radziemski, L. J., & Cremers, D. A. (1989). *Lasers-Induced Plasmas and Applications*. New York: CRC Press.

[4] Miziolek, A. W., Palleschi, V., & Schechter I. (2006). *Laser Induced Breakdown Spectroscopy*. Cambridge: Cambridge University Press.

[5] Noll, R. (2012). *Laser-Induced Breakdown Spectroscopy: Fundamentals and Applications*. New York: Springer.

[6] Harmon, R. S., Russo, R. E., & Hark, R. R. (2013). Applications of laser induced breakdown spectroscopy for geochemical and environmental analysis: A comprehensive review. *Spectrochimica Acta - Part B Atomic Spectroscopy*, *87*, 11-26.

[7] Skoog, D. A., West, D. M., Holler, F. J., & Crouch, S. R. (2004). *Fundamentals of Analytical Chemistry*. California: Cengage Learning, Inc.

[8] Fantoni, R., Caneve, L., Colao, F., Fornarini, L., Lazic, V., & Spizzichino, V. (2008). Methodologies for laboratory Laser Induced Breakdown Spectroscopy semi-quantitative and quantitative analysis-A review. *Spectrochimica Acta - Part B Atomic Spectroscopy*, *63*(10), 1097-1108.

[9] Lazic, V., Fantoni, R., Colao, F., Santagata, A., Morone, A., &

Spizzichino, V. (2004). Quantitative laser induced breakdown spectroscopy analysis of ancient marbles and corrections for the variability of plasma parameters and of ablation rate. *Journal of Analytical Atomic Spectrometry*, *19*, 429-436.

[10] El Haddad, J., Canioni, L., & Bousquet, B. (2014). Good practices in LIBS analysis: Review and advices. *Spectrochimica Acta - Part B Atomic Spectroscopy*, *101*, 171-182.

[11] Rehse, S. J., Salimnia, H., & Miziolek, A. W. (2012). Laser-induced breakdown spectroscopy (LIBS): an overview of recent progress and future potential for biomedical applications. *Journal of Medical Engineering & Technology*, *36*(2), 77–89.

[12] Taranovich, S. (2012, September 07). Mars Curiosity Rover: ChemCam laser-induced breakdown spectroscopy unveiled. Retrieved March 23, 2016, from http://www.edn.com/electronics-blogs/mission-to-mars--nasa-engineering-and-the-red-planet-/4395688/Mars-Curiosity-Rover--ChemCam-laser-induced-breakdown-spectroscopy--LIBS--unveiled

[13] Greicius, T. (2015, July 31). Curiosity Overview. Retrieved March 23, 2016, from https://www.nasa.gov/mission_pages/msl/overview/index.html

[14] Vadillo, J. M., & Laserna, J. J. (1996). Laser-induced breakdown spectroscopy of silicate, vanadate and sulfide rocks. *Talanta*, *43*(7), 1149-1154.

[15] Spizzichino, V., & Fantoni, R. (2014). Laser Induced Breakdown Spectroscopy in archeometry: A review of its application and future perspectives. *Spectrochimica Acta – Part B Atomic Spectroscopy*, *99*, 201-209.

[16] Sharma, S. K., Misra, A. K., Lucey, P. G., & Lentz, R. C. F. (2009). A combined remote Raman and LIBS instrument for characterizing minerals

with 532 nm laser excitation. *Spectrochimica Acta - Part A: Molecular and Biomolecular Spectroscopy*, *73*(3), 468–476.

[17] Muşkara, Ü. (2013). *Characterization Of Emecik Limestone Figurines For Provenance* (Unpublished doctoral thesis). Middle East Technical University, Ankara, Turkey.

[18] Rubahn, H. G. (1999). *Laser Applications in Surface Science and Technology*. Chichester: John Wiley & Sons, Ltd.

[19] Hecht, J. (2008). *Understanding Lasers: An Entry-Level Guide*. New Jersey: Wiley-IEEE Press.

[20] Koechner, W. & Bass, M. (2003). *Solid-State Lasers: A Graduate Text*. New York: Springer.

[21] Fan, T. Y. (1990). Diode-Pumped Solid State Lasers. *The Lincoln Laboratory Journal*, *3*(3), 413–426.

[22] Kim, Y. W., Cremers, D. A., & Radziemski, L. J. (1989). *Laser-Induced Plasmas and Applications*. New York: CRC Press.

[23] The National Institute of Standards and Technology (NIST) (2015, May 19). Handbook of Basic Atomic Spectroscopic Data. Retrieved April 21, 2016, from http://www.nist.gov/pml/data/handbook/index2.cfm

[24] Meggers, W. F. (1941). Notes on the Physical Basis for Spectrographic Analysis. *Journal of the Optical Society of America*, *31*(1), 39-46.

[25] Meggers, W. F. (1941). The Strongest Lines of Singly Ionized Atoms. *Journal of the Optical Society of America*, *31*(10), 605-611.

[26] The National Institute of Standards and Technology (NIST) (2014, October 8). National Standard Reference Data Series (NSRDS). Retrieved April 21, 2016, from http://www.nist.gov/srd/nsrds.cfm

[27] The National Institute of Standards and Technology (NIST) (2015, May 19). Basic Atomic Spectroscopic Data. Retrieved May 18, 2016, from http://physics.nist.gov/PhysRefData/Handbook/Tables/magnesiumtable3.htm

[28] The National Institute of Standards and Technology (NIST) (2015, May 19). Basic Atomic Spectroscopic Data. Retrieved May 18, 2016, from http://physics.nist.gov/PhysRefData/Handbook/Tables/strontiumtable4.htm

[29] The National Institute of Standards and Technology (NIST) (2015, May 19). Basic Atomic Spectroscopic Data. Retrieved May 18, 2016, from http://physics.nist.gov/PhysRefData/Handbook/Tables/chromiumtable3.htm

APPENDIX A

THE NUMERICAL VALUES FOR THE CALIBRATION CURVES

Calibration Curves for Mg (I) at 517 nm [Peak Intensity] for Figure 4.8

Sample	Concentration (mg/kg) of Constituent Mg	Peak Intensity (a.u.) of Mg (I) at 517 nm
K1	0.60	643.86
K2	0.84	1566.43
AKYA4	3.32	2298.99
KRC1	4.55	3024.34

Slope of the calibration curve = 500.02

Sample	Concentration (mg/kg) of Constituent Mg	Predicted Concentration
K1	0.60	1.29
K2	0.84	3.13
AKYA4	3.32	4.60
KRC1	4.55	6.05

$$\text{Predicted Concentration} = \text{Peak Intensity (a.u.) of Mg (I) at 517 nm} \,/_{500.02}$$

Sample	Concentration (mg/kg) of Constituent Mg	Predicted Concentration	Background Intensity
K1	0.60	0.00050	1278850
K2	0.84	0.00096	1627116
AKYA4	3.32	0.00201	1141761
KRC1	4.55	0.00212	1428517

$$\text{Predicted Concentration} = \text{Peak Intensity (a.u.) of Mg (I) at 517 nm} \,/_{Background\ Intensity}$$

Sample	Concentration (mg/kg) of Constituent Mg	Predicted Concentration	OH Emission Band Area
K1	0.60	0.03013	21369.67
K2	0.84	0.04966	31546.15
AKYA4	3.32	0.13992	16431.24
KRC1	4.55	0.13642	22170.20

$$\text{Predicted Concentration} = \text{Peak Intensity (a.u.) of Mg (I) at 517 nm} \,/_{OH\ Emission\ Band\ Area}$$

Calibration Curves for Mg (I) at 517 nm [Area Under Peak] for Figure 4.9

Sample	Concentration (mg/kg) of Constituent Mg	Area Under Peak (a.u.) of Mg (I) at 517 nm
K1	0.60	5965.48
K2	0.84	13240.34
AKYA4	3.32	17009.16
KRC6	4.55	41973.20

Slope of the calibration curve = 7208.30

Sample	Concentration (mg/kg) of Constituent Mg	Predicted Concentration
K1	0.60	0.82759
K2	0.84	1.83682
AKYA4	3.32	2.35966
KRC6	4.55	5.82290

Predicted Concentration = Area Under Peak (a.u.) of Mg (I) at 517 nm $/_{7208.30}$

Sample	Concentration (mg/kg) of Constituent Mg	Predicted Concentration	Background Intensity
K1	0.60	0.00467	1278850
K2	0.84	0.00814	1627116
AKYA4	3.32	0.01490	1141761
KRC6	4.55	0.02529	1659434

Predicted Concentration = Area Under Peak (a.u.) of Mg (I) at 517 nm $/_{Background\ Intensity}$

Sample	Concentration (mg/kg) of Constituent Mg	Predicted Concentration	OH Emission Band Area
K1	0.60	0.27916	21369.67
K2	0.84	0.41971	31546.15
AKYA4	3.32	1.03517	16431.24
KRC6	4.55	1.81309	23150.14

Predicted Concentration = Area Under Peak (a.u.) of Mg (I) at 517 nm $/_{OH\ Emission\ Band\ Area}$

Calibration Curves for Sr (II) at 421 nm [Peak Intensity] for Figure 4.10

Sample	Concentration (mg/kg) of Constituent Mg	Peak Intensity (a.u.) of Sr (II) at 421 nm
K1	628	1189.13
FIGURINE4	711	2811.51
K2	915	3435.26

Slope of the calibration curve = 6.93

Sample	Concentration (mg/kg) of Constituent Mg	Predicted Concentration
K1	628	171.67
FIGURINE4	711	405.89
K2	915	495.94

Predicted Concentration = Peak Intensity (a.u.) of Sr (II) at 421 nm $/_{6.93}$

Sample	Concentration (mg/kg) of Constituent Mg	Predicted Concentration	Background Intensity
K1	628	0.00093	1278850
FIGURINE4	711	0.00162	1738174
K2	915	0.00211	1627116

Predicted Concentration = Peak Intensity (a.u.) of Sr (II) at 421 nm $/_{Background\ Intensity}$

Sample	Concentration (mg/kg) of Constituent Mg	Predicted Concentration	OH Emission Band Area
K1	628	0.05565	21369.67
FIGURINE4	711	0.07168	39224.08
K2	915	0.10890	31546.15

Predicted Concentration = Peak Intensity (a.u.) of Sr (II) at 421 nm $/_{OH\ Emission\ Band\ Area}$

Calibration Curves for Sr (II) at 421 nm [Area Under Peak] for Figure 4.11

Sample	Concentration (mg/kg) of Constituent Mg	Area Under Peak (a.u.) of Sr (II) at 421 nm
K1	628	7848.99
FIGURINE4	711	20297.03
K2	915	23938.21

Slope of the calibration curve = 48.85

Sample	Concentration (mg/kg) of Constituent Mg	Predicted Concentration
K1	628	160.67
FIGURINE4	711	415.47
K2	915	490.01

$$\text{Predicted Concentration} = \text{Area Under Peak (a.u.) of Sr (II) at 421 nm} / _{48.85}$$

Sample	Concentration (mg/kg) of Constituent Mg	Predicted Concentration	Background Intensity
K1	628	0.00614	1278850
FIGURINE4	711	0.01168	1738174
K2	915	0.01471	1627116

$$\text{Predicted Concentration} = \text{Area Under Peak (a.u.) of Sr (II) at 421 nm} / _{Background\ Intensity}$$

Sample	Concentration (mg/kg) of Constituent Mg	Predicted Concentration	OH Emission Band Area
K1	628	0.36730	21369.67
FIGURINE4	711	0.51746	39224.08
K2	915	0.75883	31546.15

$$\text{Predicted Concentration} = \text{Area Under Peak (a.u.) of Sr (II) at 421 nm} / _{OH\ Emission\ Band\ Area}$$

Calibration Curves for Cr (I) at 428 nm [Peak Intensity] for Figure 4.12

Sample	Concentration (mg/kg) of Constituent Mg	Peak Intensity (a.u.) of Cr (I) at 428 nm
K1	45.40	441.02
AKYA4	344	1099.72
RZG2	593	790.05
KRC6	785	1992.81

Slope of the calibration curve = 1.70

Sample	Concentration (mg/kg) of Constituent Mg	Predicted Concentration
K1	45.40	260.27
AKYA4	344	649
RZG2	593	466.24
KRC6	785	1176.05

Predicted Concentration = Peak Intensity (a.u.) of Cr (I) at 428 nm $/_{1.70}$

Sample	Concentration (mg/kg) of Constituent Mg	Predicted Concentration	Background Intensity
K1	45.40	0.00035	1278850
AKYA4	344	0.00096	1141761
RZG2	593	0.00075	1047733
KRC6	785	0.00120	1659434

Predicted Concentration = Peak Intensity (a.u.) of Cr (I) at 428 nm $/_{Background\ Intensity}$

Sample	Concentration (mg/kg) of Constituent Mg	Predicted Concentration	OH Emission Band Area
K1	45.40	0.02064	21369.67
AKYA4	344	0.06693	16431.24
RZG2	593	0.06747	11709.94
KRC6	785	0.08608	23150.14

Predicted Concentration = Peak Intensity (a.u.) of Cr (I) at 428 nm $/_{OH\ Emission\ Band\ Area}$

Calibration Curves for Cr (I) at 428 nm [Area Under Peak] for Figure 4.13

Sample	Concentration (mg/kg) of Constituent Mg	Area Under Peak (a.u.) of Cr (I) at 428 nm
K1	45.40	4983.91
AKYA4	344	9943.89
RZG2	593	7889.39
KRC6	785	20705.64

Slope of the calibration curve = 17.40

Sample	Concentration (mg/kg) of Constituent Mg	Predicted Concentration
K1	45.40	286.38
AKYA4	344	571.39
RZG2	593	453.34
KRC6	785	1189.77

Predicted Concentration = Area Under Peak (a.u.) of Cr (I) at 428 nm $/_{17.40}$

Sample	Concentration (mg/kg) of Constituent Mg	Predicted Concentration	Background Intensity
K1	45.40	0.00390	1278850
AKYA4	344	0.00871	1141761
RZG2	593	0.00753	1047733
KRC6	785	0.01248	1659434

Predicted Concentration = Area Under Peak (a.u.) of Cr (I) at 428 nm $/_{Background\ Intensity}$

Sample	Concentration (mg/kg) of Constituent Mg	Predicted Concentration	OH Emission Band Area
K1	45.40	0.23322	21369.67
AKYA4	344	0.60518	16431.24
RZG2	593	0.67373	11709.94
KRC6	785	0.89441	23150.14

Predicted Concentration = Area Under Peak (a.u.) of Cr (I) at 428 nm $/_{OH\ Emission\ Band\ Area}$